BABEȘ-BOLYAI UNIVERSITY
FACULTY OF PHYSICS

# Implementation of Gold Nano-Bipyramids as Efficient Biosensing Enhancers and Thermo-Plasmonic Generators

By

**CÂMPU ANDREEA-MARIA**

**PhD. Thesis Summary**

SCIENTIFIC ADVISORS
**Prof. Univ. Dr. SIMION AȘTILEAN**

CLUJ-NAPOCA
2020

# ***Table of contents***

## Motivation and outline

The nanotechnology research field is in constant progress aiming to meet the needs of the society's high impact industries and communities from technical domains to biological and medical applications. One of the main concerns of the scientific community is represented by the healthcare system, specifically the need of a low-cost, effective, and proper care. Thus, a lot of effort is driven towards finding the best approaches to prevent, early detect and efficiently treat life-threatening diseases.

In this scientific context, the development of simple, affordable, and accurate nano-systems in view of their implementation in medical applications are of high interest. For this purpose, gold nanoparticles have gathered a lot of attention due to their unique optical properties strongly related to the great variety of sizes and shapes. However, a less studied geometry is the nano-bipyramidal morphology, which due to its sharp tips and edges holds promising advantages for both biosensing and therapy applications. Therefore, in this work, we aim to analyse and determine the features exhibited by these elongated sharp nanoparticles and further exploit them aspiring to answer to the nanotechnological demands of the biomedical diagnosis and therapy community, specifically, the ease-of-use and simple manipulation, high biocompatibility and stability, short reaction time, high specificity and selectivity, enhancing abilities and simultaneous multimodal application.

To have an overall view of the gold nanoparticles' theoretical considerations and their already known and well-described features available in literature, Chapter I introduces and analytically discusses their properties and plasmon-induced effects, highlighting thus their impact on several analysis techniques as well as therapeutic approaches.

Chapter II is designated to the synthesis of the gold nano-bipyramidal nanoparticles (AuBPs), pointing out the advantages and challenges encountered on the way to control the fabrication of such elongated nanostructures with finely tuneable optical responses. Their thorough optical and morphological characterisation is described along with the evaluation of their sensitivity.

Chapter III presents three different biosensing designs which take advantage of the AuBPs' role as efficient active nano-antennas. Considering the strong biotin-streptavidin recognition interaction, the "proof-of-concept" was demonstrated first for the AuBPs in solution proving their capability to operate as an immunosensor enabling the multimodal detection of target analytes. Next, a paper-based plasmonic nanoplatform was designed by an innovative calligraphy approach, which allows the fabrication of spatially isolated

plasmonic lines, thus determining its multiplexing abilities. The dual detection of molecules of interest was realized by complementary techniques proving its versatility as efficient, inexpensive, flexible, portable, and miniaturized Point-of-Care device. Lastly, a microfluidic integrated plasmonic biosensing device was developed allowing thus the 3D volumetric detection of analytes at ultra-low concentrations.

Chapter IV is focused on the non-radiative features of the AuBPs, specifically the determination of their intrinsic photothermal and photodynamic properties under two near infrared excitation laser lines. The promising and exciting results obtained have further led to the development of a hybrid AuBPs'-based nano-system having a photosensitizer (PS) incorporated, thus the nanostructures were proven to significantly enhance the PS's therapeutic activity. The dual photothermal and photodynamic therapy was then practically validated on epithelial melanoma cells.

To summarize, Chapter V comprises the final and most important conclusions drawn after each study as well as the proposed future work.

All the results obtained throughout this thesis were valorised by their publication in high impact factor journals and presented at international conferences.

**Keywords:** Gold nano-bipyramids, Synthesis, Multimodal biodetection, Multiplexed detection, Intrinsic photothermal properties, Intrinsic photodynamic properties, Dual photothermal and photodynamic therapy

# Abbreviations

**LSPR** – Localized Surface Plasmon Resonance

**SPR** – Surface Plasmon Resonance

**SERS** – Surface Enhanced Raman Spectroscopy

**SEIRA** – Surface Enhanced Infrared Absorption

**MEF** – Metal Enhanced Fluorescence

**PTT** – Photothermal Therapy

**PDT** – Photodynamic Therapy

**ROS** – Reactive Oxygen Species

**PS** – Photosensitizer

**NIR** – Near Infrared

**IR** – Infrared

**UV -** Ultraviolet

**AuBPs** – Gold nano-bipyramids

**AuNRs** – Gold nanorods

**AR** – Aspect Ratio

**RIS** – Refractive Index Sensitivity

**RI** – Refractive Index

**FWHM** – Full-Width at Half Maximum

**FOM** – Figure of Merit

**LOD** – Limit of Detection

**POC** – Point-of-Care

**LOC** – Lab-on-a-Chip

**DLS** – Dynamic Light Scattering

**TEM** – Transmission Electron Microscopy

**HR-TEM** – High Resolution Transmission Electron Microscopy

**SEM** – Scanning Electron Microscopy

**TLC** – Thin-Layer Chromatography

**FT-IR** – Fourier-Transform Infrared Spectroscopy

**DFT** – Discrete Fourier Transform

**FDTD -** Finite-Difference Time-Domain

**TFSF** – Total Field Scattered Field

**EM** – Electromagnetic Field

# Chapter I. Introduction to gold nanoparticles and plasmon-based applications

## I.1 Gold nanoparticles

A lot of research is currently revolved around gold nanoparticles and has been for the past years, however they were already employed in the ancient times. The very first application was in glass colouring [1] to obtain the beautiful stained glasses we get to admire at buildings and objects, which were preserved through time and history. Nowadays, gold nanoparticles are considered of high interest for a large variety of applications such as diagnostic tools, detection devices, contrast, and/or therapeutic agents by exploiting their unique properties.

## I.2 Optical properties of gold nanoparticles

Gold nanoparticles, due to their nano-meter size exhibit unique optical properties [2]. The absorption characteristics are given by the so-called localized surface plasmon resonance (LSPR) bands, which result from the collective oscillations of the conduction electrons upon the resonant excitation by an electromagnetic light source (Figure I.1.2.1.). The phenomenon was firstly described by the Mie theory [3], which addresses the simple case of a gold nanosphere and determines that the extinction spectrum is composed of both the absorption and scattering of light by a material. However, by solving Maxwell's equations [4], the LSPR band is proven to be sensitive to the microenvironment along with its dependency on shape and size. Furthermore, gold nanostructures generate an enhanced electromagnetic field inducing thus changes to the nanoparticles' surrounding microenvironment promoting the Raman or fluorescence phenomena [5].

[1] Marie-Christine Daniel and Didier Astruc, "Gold Nanoparticles: Assembly, Supramolecular Chemistry, Quantum-Size-Related Properties, and Applications toward Biology, Catalysis, and Nanotechnology," *Chemical Reviews* 104, no. 1 (January 1, 2004): 293–346, https://doi.org/10.1021/cr030698+.
[2] K. Kaur, "Optical Biosensing Using Localized Surface Plasmon Resonance of Gold Nanoparticles" (University of Waterloo, Canada, 2011).
[3] Gustav Mie, "Beiträge zur Optik trüber Medien, speziell kolloidaler Metallösungen," *Annalen der Physik* 330, no. 3 (1908): 377–445, https://doi.org/10.1002/andp.19083300302.
[4] Daniel and Astruc, "Gold Nanoparticles: Assembly, Supramolecular Chemistry, Quantum-Size-Related Properties, and Applications toward Biology, Catalysis, and Nanotechnology."
[5] M. Iosin et al., "Study of Protein–Gold Nanoparticle Conjugates by Fluorescence and Surface-Enhanced Raman Scattering," *Journal of Molecular Structure* 924–926 (April 2009): 196–200, https://doi.org/10.1016/j.molstruc.2009.02.004.

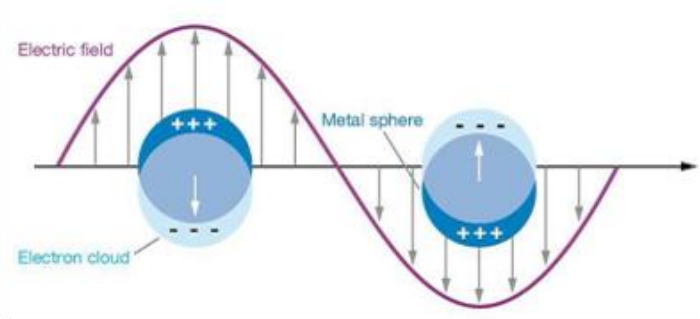


**Figure I.2.** Schematic illustration of the Surface Plasmon Resonance phenomenon in the simple case of the gold nanospheres.

Plasmonic LSPR-based nano-sensors have been regarded as efficient detection tools, Sharma et al. provide a review summing up variety of target analytes successfully evidenced by LSPR with limits of detection up to 350 fM [6]. By the functionalization of the nanoparticles with specific molecules, the detection of target analytes is enabled up to 0.1 aM [7]. Jean-Francois Masson reviews the applicability of SPR/LSPR biosensors in clinical applications revealing the utility of the LSPR designs for clinical purposes [8] as well as environment, food and agriculture and detection of volatile gases [9].

### I.2.1 Surface enhanced Raman spectroscopy (SERS)

The Raman spectroscopy represents an important vibrational analysis technique, which allows the identification of molecules based on their chemical structure due to its "fingerprinting" capabilities. The Raman effect is described by the classical electromagnetic theory: as a result of the interaction of an incident light source with a polarizable molecule, the latter becomes an oscillation dipole, which, subsequently, reemits or scatters light having the same frequency as the dipole oscillation.

The Raman effect is a very weak phenomenon, fluorescence, in comparison, is 6 to 10 orders of magnitude stronger [10]. In this context, to overcome this major drawback, the molecules are placed near a metallic surface in order to enhance the Raman signal. This effect is the so-called Surface Enhanced Raman Scattering (SERS). SERS was firstly observed in 1974 by Fleischmann, Hendra and McQuillan, who have remarked that the

[6] Shubhanshi Sharma et al., "Optical Biosensing with Electromagnetic Nanostructures," *Reviews in Physics* 5 (November 2020): 100044, https://doi.org/10.1016/j.revip.2020.100044.
[7] Yuanyuan Tian, Lei Zhang, and Lianhui Wang, "DNA-Functionalized Plasmonic Nanomaterials for Optical Biosensing," *Biotechnology Journal* 15, no. 1 (January 2020): 1800741, https://doi.org/10.1002/biot.201800741.
[8] Jean-Francois Masson, "Surface Plasmon Resonance Clinical Biosensors for Medical Diagnostics," *ACS Sensors* 2, no. 1 (January 27, 2017): 16–30, https://doi.org/10.1021/acssensors.6b00763.
[9] Jean-Francois Masson, "Portable and Field-Deployed Surface Plasmon Resonance and Plasmonic Sensors," *The Analyst* 145, no. 11 (2020): 3776–3800, https://doi.org/10.1039/D0AN00316F.
[10] Eric C. Le Ru and Pablo G. Etchegoin, *Principles of Surface-Enhanced Raman Spectroscopy: And Related Plasmonic Effects*, 1st ed (Amsterdam ; Boston: Elsevier, 2009).

roughness of the silver electrode surface influences the intensity of the Raman signal of the pyridine molecule [11]. To date, studies report the amplification of the Raman signal with $10^{10}$ to $10^{11}$ orders of magnitude. To describe the SERS mechanism, the scientific community accepted to two theories [12]: the electromagnetic enhancement (EM) and chemical mechanism (CM), respectively.

EM is related to the substrate and independent of the absorbate, it arises due to the resonant photoexcitation of the surface plasmons of the metallic surface and, thus, inducing a significant amplification of the electromagnetic field [13].

In contrast, CM arises from the interaction of the absorbate with the metallic surface, mainly the charge transfer between the two entities which results into changes in the molecules polarizability [14].

Conventionally, SERS substrates are realized by depositing metallic nanoparticles onto a solid support, thus the roughness of the surface is achieved. Recently, much more exciting designs proving flexibility and transparency have been developed for efficient SERS employment. The flexible and eco-friendly cellulose-based substrates, most commonly used is filter paper, have gathered a lot of attention, Ogundare and van Zyl offer a great overview of their development and applicability in bioanalysis reaching limits of detection up to 100 fM [15]. The combination of gold-silver alloy nanoparticles and silica matrices for the development of SERS efficient substrates was proven to be reliable for the detection of explosives reaching limits of detection of nanomolar [16]. Supports of polymeric nature are no strangers to the adsorption of nanoparticles for flexible and transparent SERS substrate development [17]. An additional advantage of the SERS technique is highlighted by Sun et al., specifically the benefit of the on-site analysis implementation using various SERS-active substrates [18].

---

[11] M. Fleischmann, P. J. Hendra, and A. J. McQuillan, "Raman Spectra of Pyridine Adsorbed at a Silver Electrode," *Chemical Physics Letters* 26, no. 2 (May 15, 1974): 163–66, https://doi.org/10.1016/0009-2614(74)85388-1.

[12] Cheng Zong et al., "Surface-Enhanced Raman Spectroscopy for Bioanalysis: Reliability and Challenges," *Chemical Reviews* 118, no. 10 (May 23, 2018): 4946–80, https://doi.org/10.1021/acs.chemrev.7b00668.

[13] George C Schatz and Richard P Van Duyne, "Handbook of Vibrational Spectroscopy," *New York: Wiley* 1 (2002): 759; P. Alonso-González et al., "Resolving the Electromagnetic Mechanism of Surface-Enhanced Light Scattering at Single Hot Spots," *Nature Communications* 3, no. 1 (January 2012): 684, https://doi.org/10.1038/ncomms1674;
Song-Yuan Ding et al., "Nanostructure-Based Plasmon-Enhanced Raman Spectroscopy for Surface Analysis of Materials," *Nature Reviews Materials* 1, no. 6 (June 2016): 16021, https://doi.org/10.1038/natrevmats.2016.21.

[14] Pilot et al., "A Review on Surface-Enhanced Raman Scattering," *Biosensors* 9, no. 2 (April 17, 2019): 57, https://doi.org/10.3390/bios9020057.

[15] Segun A. Ogundare and Werner E. van Zyl, "A Review of Cellulose-Based Substrates for SERS: Fundamentals, Design Principles, Applications," *Cellulose* 26, no. 11 (July 2019): 6489–6528, https://doi.org/10.1007/s10570-019-02580-0.

[16] Sree Satya Bharati Moram et al., "Instantaneous Trace Detection of Nitro-Explosives and Mixtures with Nanotextured Silicon Decorated with Ag–Au Alloy Nanoparticles Using the SERS Technique," *Analytica Chimica Acta* 1101 (March 2020): 157–68, https://doi.org/10.1016/j.aca.2019.12.026.

[17] Zhuoyao Li, Xiao Huang, and Gang Lu, "Recent Developments of Flexible and Transparent SERS Substrates," *Journal of Materials Chemistry C* 8, no. 12 (2020): 3956–69, https://doi.org/10.1039/D0TC00002G.

[18] Ji Sun et al., "Surface-enhanced Raman Spectroscopy for On-site Analysis: A Review of Recent Developments," *Luminescence*, March 11, 2020, bio.3796, https://doi.org/10.1002/bio.3796.

### I.2.2 Surface enhanced infra-red absorption spectroscopy (SEIRA)

The Surface Enhanced Infra-Red Absorption Spectroscopy (SEIRA) is a sensitive surface analysis technique which takes advantage of the electromagnetic properties of the metallic nanoparticles similarly as SERS. The mechanism of SEIRA is nicely described by Heberle and Ataka, who discuss the two theories associated with the noticed surface enhancement: electromagnetic field enhancement and mixed effective medium [19]. The principle of the technique relies on the excitation of the composite medium and, subsequently, the coupling of the oscillating dipole of the molecules with the oscillations of the surface conduction electrons of the metal leading to a higher overall absorbance. the technique does not only allow the detection of adsorbed molecules, but also enables the determination of their orientation with respect to the metallic surface [20]. The signal amplification can reach $10^3 – 10^6$ orders of magnitude, thus proving the high sensitivity of the technique [21] leading towards atto-molar limit of detection [22].

### I.2.3 Metal enhanced fluorescence (MEF)

Even though the Metal Enhanced Florescence (MEF) was firstly observed in 1974 [23], the phenomenon was thoroughly studied and described by Lakowicz [24]. MEF arises as a result of the interaction between fluorophores in the excited state and the surface plasmon resonances exhibited by the metals. The excited fluorophores act as oscillating dipoles to which the metal responds by modifying the emission rates and the spatial distribution of the radiated energy. The interaction between the metal with both the incident light and the fluorophore induces changes in the electric field felt by the latter. On the other hand, the fluorophore alike generates a field in the metal. As a result of these interactions, the field incident on the fluorophore and the radiative decay rates can be increased or decreased. The increase of the radiative decay rate can be explained by the Jablonksi diagram (Figure I.2.3.) taking into consideration the behaviour of the fluorophore without and with the metal. In the presence of the metal, the additional excitation rate ($E_m$) assigned to the metal

[19] Joachim Heberle and Kenichi Ataka, "Surface Enhanced Infrared Absorption Spectroscopy," in *Encyclopedia of Biophysics*, ed. Gordon C. K. Roberts (Berlin, Heidelberg: Springer Berlin Heidelberg, 2013), 2528–31, https://doi.org/10.1007/978-3-642-16712-6_127.
[20] Masatoshi Osawa, "Surface-Enhanced Infrared Absorption," in *Near-Field Optics and Surface Plasmon Polaritons*, ed. Satoshi Kawata, vol. 81, Topics in Applied Physics (Berlin, Heidelberg: Springer Berlin Heidelberg, 2001), 163–87, https://doi.org/10.1007/3-540-44552-8_9.
[21] R. Adato et al., "Ultra-Sensitive Vibrational Spectroscopy of Protein Monolayers with Plasmonic Nanoantenna Arrays," *Proceedings of the National Academy of Sciences* 106, no. 46 (November 17, 2009): 19227–32, https://doi.org/10.1073/pnas.0907459106.
[22] Hang Yin et al., "Gold Nanonails for Surface-Enhanced Infrared Absorption," *Nanoscale Horizons*, 2020, 10.1039.D0NH00244E, https://doi.org/10.1039/D0NH00244E.
[23] K. H. Drexhage, "Progress in Optics XII," *Progress in Optics (North-Holland, Amsterdam, 1974)*, 1974.
[24] Joseph R. Lakowicz, *Principles of Fluorescence Spectroscopy*, Third edition, corrected at 4. printing (New York, NY: Springer, 2010).

increases the radiative decay by adding a new radiative decay rate ($\Gamma_m$) arisen from the metal.

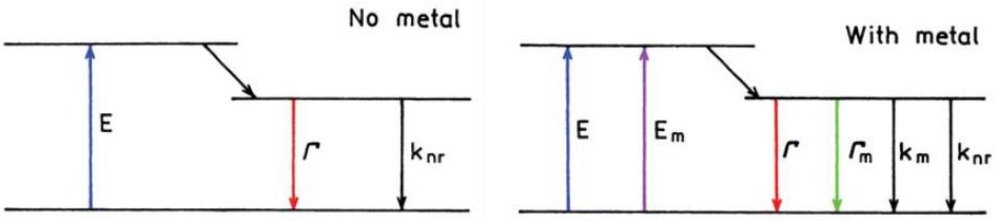


**Figure I.2.3.** The Jablonski diagram describing the fluorescence emission in the absence (left) and presence (right) of the metal surfaces.

## I.3 Therapeutic effects for biomedical applications

Advances are being made to find not only bio-detection tools for early diagnostics, but also effective treatments for, at the moment, incurable or high-risk diseases. One of these worldwide health threats is cancer. To date, the most common therapeutic approaches include surgery, (bio)chemotherapy, immunotherapy and, more recently, the photodynamic therapy was considered for clinical trials [25]. However, due to their limitations and side effects, a lot of the scientific effort is put into the development of therapeutic applications based on (bio)materials with improved specificity, biocompatibility, targeting capabilities and localized distribution at the tumorous site, thus aiming to replace the current invasive cancer treatment strategies [26].

Plasmonic nanoparticles represent a class of nano-systems worth exploiting. Metallic nanostructures were demonstrated to play an important role in innovative cancer treatment strategies [27]. Efficient therapeutic agents were developed showing multi-modal activation: (i) internal stimulation by factors like pH, temperature [28] and (ii) external

[25] Beatriz Domingues et al., "Melanoma Treatment in Review," *ImmunoTargets and Therapy* 7 (2018): 35–49, https://doi.org/10.2147/ITT.S134842.
[26] M.A. Stokman et al., "Preventive Intervention Possibilities in Radiotherapy- and Chemotherapy-Induced Oral Mucositis: Results of Meta-Analyses," *Journal of Dental Research* 85, no. 8 (August 2006): 690–700, https://doi.org/10.1177/154405910608500802;
Carole Soussain et al., "CNS Complications of Radiotherapy and Chemotherapy," *The Lancet* 374, no. 9701 (November 2009): 1639–51, https://doi.org/10.1016/S0140-6736(09)61299-X;
Shihao Yang et al., "Autoimmune Effects of Lung Cancer Immunotherapy Revealed by Data-Driven Analysis on a Nationwide Cohort," *Clinical Pharmacology & Therapeutics* 107, no. 2 (February 2020): 388–96, https://doi.org/10.1002/cpt.1597;
Martine J. Sealy et al., "Low Muscle Mass Is Associated with Early Termination of Chemotherapy Related to Toxicity in Patients with Head and Neck Cancer," *Clinical Nutrition* 39, no. 2 (February 2020): 501–9, https://doi.org/10.1016/j.clnu.2019.02.029.
[27] Zhixuan Song et al., "Mesoporous Silica-Coated Gold Nanorods with a Thermally Responsive Polymeric Cap for near-Infrared-Activated Drug Delivery," *Journal of Materials Science* 53, no. 10 (May 2018): 7165–79, https://doi.org/10.1007/s10853-018-2117-7.
[28] Wei Li et al., "Overcoming Photodynamic Resistance and Tumor Targeting Dual-Therapy Mediated by Indocyanine Green Conjugated Gold Nanospheres," *Journal of Controlled Release* 258 (July 2017): 171–81, https://doi.org/10.1016/j.jconrel.2017.05.015.

triggers [29]. Furthermore, different surface modifications ensure not only improved biocompatibility and specificity by cellular recognition functionalization, but also encourage the integration of multiple functionalities onto the same platform leading to theragnostic and synergistic plasmon-assisted Photothermal (PTT) and Photodynamic (PDT) therapeutic nanoplatforms as reports are found in the specialty literature [30].

### I.3.1 Photothermal effect

The photothermal effect is described by a series of waterfall-phenomena induced by the absorption of light, specifically by the resonant photoexcitation of the electron cloud, and leading towards thermal dissipation. Firstly, as the photons are absorbed the particles start to oscillate and, thus, the non-thermal charge distribution is induced thermalizing *via* elastic electron-electron scattering until an equilibrium Fermi electron distribution correlating with higher electron temperatures is reached. Thereby, the temperature of the surface rapidly increases. The cooling of the Fermi distribution is associated to an electron-phonon coupling process, which brings the system to an equilibrium state leading to the formation of the hot metallic lattice. The following phonon-phonon interactions enable the heat dissipation at the particle-surrounding microenvironment interface [31].

### I.3.2 Photodynamic effect

The photodynamic therapy (PDT) is based on a straightforward concept of applicability with the aim to induce efficient cancerous cells death in a targeted manner, thus sparing the healthy tissue. The mechanism relies on the photoexcitation of the PS, which, subsequently, crosses from the ground state ($S_0$) to an excited state ($S_1$). The relaxation of the PS back to the ground energy state is realized radiatively by fluorescence

[29] Wei Li et al., "Gold Nanospheres-Stabilized Indocyanine Green as a Synchronous Photodynamic–Photothermal Therapy Platform That Inhibits Tumor Growth and Metastasis," *ACS Applied Materials & Interfaces* 9, no. 4 (February 2017): 3354–67, https://doi.org/10.1021/acsami.6b13351.

[30] Shan Fang et al., "Dual-Stimuli Responsive Nanotheranostics for Multimodal Imaging Guided Trimodal Synergistic Therapy," *Small* 13, no. 6 (February 2017): 1602580, https://doi.org/10.1002/smll.201602580;
Na An, Huiming Lin, and Fengyu Qu, "Synthesis of a GNRs@mSiO $_2$ -ICG-DOX@Se-Se-FA Nanocomposite for Controlled Chemo-/Photothermal/Photodynamic Therapy" *European Journal of Inorganic Chemistry* 2018, no. 39 (October 24, 2018): 4375–84, https://doi.org/10.1002/ejic.201800572;
Muhammad Rizwan Younis et al., "Low Power Single Laser Activated Synergistic Cancer Phototherapy Using Photosensitizer Functionalized Dual Plasmonic Photothermal Nanoagents," *ACS Nano*, February 11, 2019, acsnano.8b09552, https://doi.org/10.1021/acsnano.8b09552;
Fangfang Xia et al., "Matrix Metallopeptidase 2 Targeted Delivery of Gold Nanostars Decorated with IR-780 Iodide for Dual-Modal Imaging and Enhanced Photothermal/Photodynamic Therapy," *Acta Biomaterialia* 89 (April 2019): 289–99, https://doi.org/10.1016/j.actbio.2019.03.008.

[31] Essraa A. Hussein et al., "Recent Advances in Functional Nanostructures as Cancer Photothermal Therapy," International Journal of Nanomedicine, May 17, 2018, https://doi.org/10.2147/IJN.S161031; Stephan Link and Mostafa A. El-Sayed, "Shape and Size Dependence of Radiative, Non-Radiative and Photothermal Properties of Gold Nanocrystals," *International Reviews in Physical Chemistry* 19, no. 3 (July 1, 2000): 409–53, https://doi.org/10.1080/01442350050034180;
D. Keith Roper, W. Ahn, and M. Hoepfner, "Microscale Heat Transfer Transduced by Surface Plasmon Resonant Gold Nanoparticles," *The Journal of Physical Chemistry C* 111, no. 9 (March 2007): 3636–41, https://doi.org/10.1021/jp064341w.

emission, through internal conversion of the light and dissipation of heat and/or the PS can further transit a temporary excited triplet state ($T_1$) through intersystem crossing inducing thus the generation of photochemical reactions and, implicitly, generation of the ROS responsible for the PDT therapy.

The high absorption capabilities of the gold nanoparticles make them intriguing in view of PDT applications. Their high stability represents an additional advantage for their implementation as enhancers of the photodynamic activity of PS.

# Chapter II. Gold nano-bipyramids – chemical synthesis and characterisation –

## II.1 Introduction

Gold nano-bipyramids (AuBPs) constitute a category of anisotropic elongated nanoparticles along with gold nanorods (AuNRs), which present similarities in shape and, subsequently, in the exhibited optical properties, both in LSPR and local electromagnetic field enhancement. The formation of these elongated shapes relies mostly on specific interactions between the capping agents, such as surfactants, ligands, polymers and others, and the different growing faces of the particles. These interactions define the morphology of the nanostructures and allow the fine tuning of their size.

## II.2 Gold nano-bipyramids – chemical synthesis and purification

Important advances in the fabrication of AuBPs were made by Narvarro et al. [32] and Chateau et al. [33], based on their reported method, an adapted version of the seed-mediated growth approach was used to chemically synthesize the AuBPs used in the proposed studies discussed in this doctoral thesis. As the name implies, the process involves two steps: (i) the synthesis of the seeds and (ii) the growth of the AuBPs from the prepared seeds.

For the growth of the AuBPs, cetyltrimethylammonium chloride (CTAC)-stabilized polycrystalline spherical seeds are produced by mixing 1 M gold (III) chloride hydrate ($HAuCl_4$) with 25 w % CTAC stabilizing agent solution at room temperature and under vigorous stirring, which afterwards is turn down to mild conditions. 0.25 M nitric acid ($HNO_3$) are added to the mixture followed by a 50 mM sodium borohydride ($NaBH_4$) solution. Subsequently, after the add-on of 1 M citric acid, the seed solution undergoes an aging treatment by thermally treating them for 60 to 90 minutes at 80 ºC, while the stirring is completely turned off.

The final step is to grow the AuBPs from the seed solution as follows: 25 mM $HAuCl_4$ were mixed with 45 mM CTAB, 5 mM $AgNO_3$ and 0.4 M HQL were then added. Lastly, various volumes of the seed solution (from 300 to 6 µL) are added to the growing solution. All reactions were performed at room temperature and immediately after each addition, the solution was gently mixed. The final solution is left undisturbed at 45 ºC for

[32] Julien R. G. Navarro et al., "Synthesis, Electron Tomography and Single-Particle Optical Response of Twisted Gold Nano-Bipyramids," *Nanotechnology* 23, no. 14 (2012): 145707, https://doi.org/10.1088/0957-4484/23/14/145707.
[33] D. Chateau et al., "From Gold Nanobipyramids to Nanojavelins for a Precise Tuning of the Plasmon Resonance to the Infrared Wavelengths: Experimental and Theoretical Aspects," *Nanoscale* 7, no. 5 (February 7, 2015): 1934–43, https://doi.org/10.1039/c4nr06323f.

50 minutes. For larger nanoparticles, the reduction agent addition procedure was slightly modified, 2/3 of the HQL volume was added as usual during the synthesis, while the remaining 1/3 was dropped after 10 to 15 minutes of the thermal treatment when the solution became light brownish in colour. For this growth approach, low seed volumes are used.

The reactants excess and potential by-products are removed as the AuBPs undergo two purification steps by centrifugation at 8000 rotations per minute (rpm) for 15 minutes and redispersion in ultrapure water with a resistivity of 18.2 mΩ.

## II.3 LSPR and TEM characterisation

In view of further use, the as-fabricated AuBPs systems were thoroughly optically and morphologically characterised. Figure II.3(a) presents digital images of the flasks containing the colloidal solutions, which change colour corresponding to their optical response from dark green to dark brown. All extinction spectra exhibit the two characteristic LSPR bands, specifically, a stationary band at around 512 nm resulted from the collective oscillations of the transversal surface conduction electrons and a narrower, more intense band, namely the longitudinal LSPR response, arisen from the longitudinal vibrations of the electron cloud. The latter optical response spans from 686 to 1107 nm (Figure II.3(b)) with respect to the nanoparticles' aspect ratio (AR). In our case, the AR values were determined based on the Transmission Electron Microscopy (TEM) images obtained for each colloidal solution (Figure II.3(c)). The microscopic images were analysed using the professional ImageJ toolkit by measuring the length and width of 100 nanostructures for each sample and statistically determining the mean values of their dimensions, which were then used to calculate the AR of each AuBPs solution. The obtained AR increase from 2.9 to 5.79 along with the higher LSPR spectral position. Dynamic Light Scattering (DLS) measurements were acquired, and the obtained hydrodynamic diameters are in good agreement with the dimensions determined based on the TEM images. Additionally, the surface charge of the AuBPs was evaluated to be + 27 mV by Zeta Potential measurements.

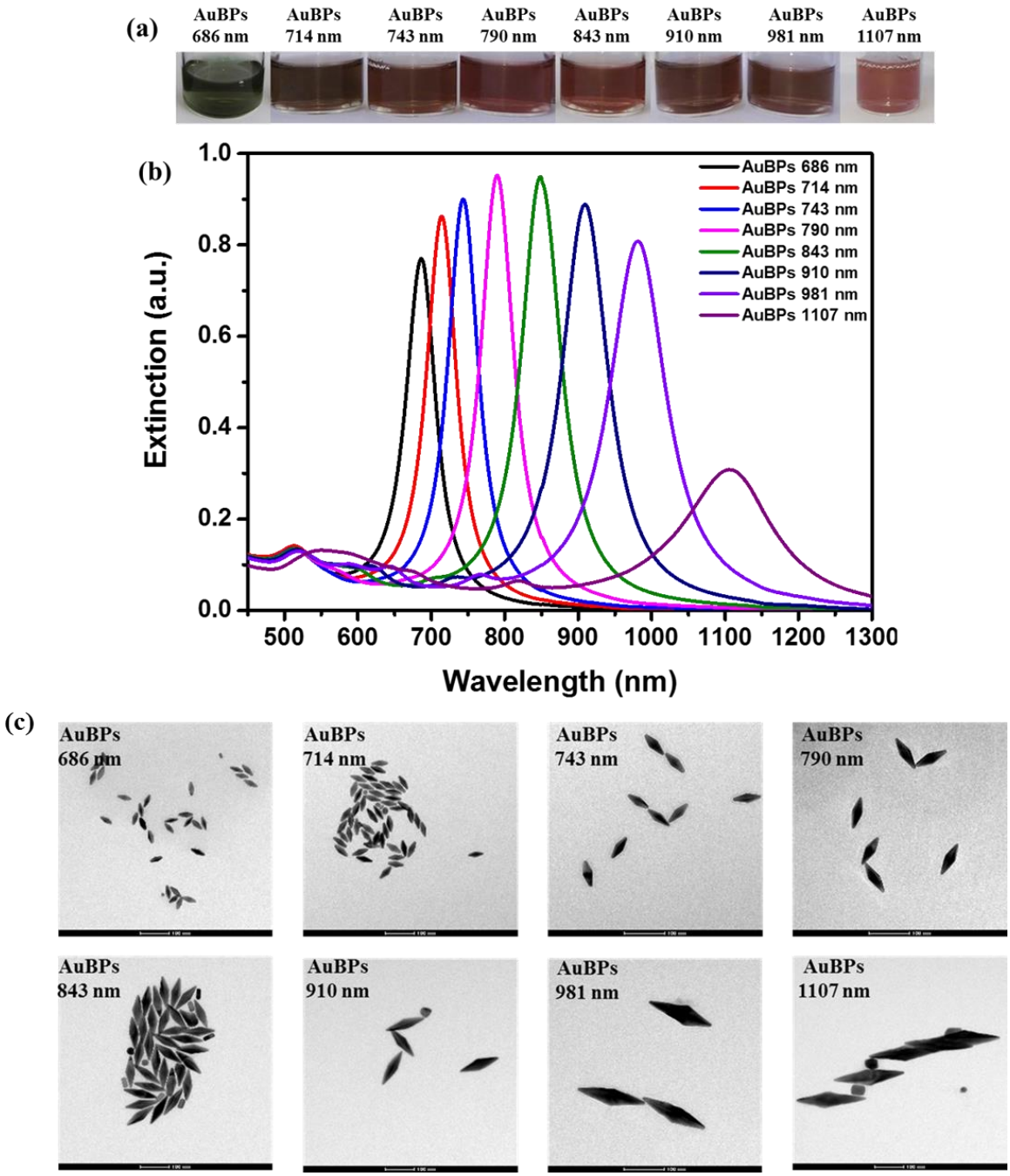


**Figure II.3. (a)** Digital images of the flasks containing the colloidal AuBPs solutions, **(b)** the corresponding extinction spectra and **(c)** TEM microscopic images of the as-synthesized AuBPs. Scale bar: 100 nm.

## II.4 *Bulk* refractive index sensitivity (RIS)

The determination of the LSPR detection capabilities of the as-synthesized AuBPs is based on the evaluation of their *bulk* refractive index sensitivity (RIS) when the refractive index (RI) of the microenvironment in the vicinity of the nanostructures' changes. The as-

synthesized AuBPs were placed in water-glycerol mixtures with known RI (from 1.333 to 1.473). The recorded extinction spectra show red-shifts of the longitudinal LSPR up to 60 nm. By plotting the recorded red-shifts of the longitudinal LSPR response of each analysed AuBPs against the RI values, the LSPR bulk sensitivity was determined to increase from 222 nm/ refractive index unit (nm/RIU) for the AuBPs with LSPR at 692 nm to 551 nm/RIU for the AuBPs with the optical response located at 972 nm.

## II.5 Conclusions

This chapter represents the stepping stone in the development of AuBPs-based hybrid nanoplatform designs for a wide field of biological applications by demonstrating the high reproducibility of the synthesis approach and the uniformity of the morphological properties proven by two complementary techniques, the stability of the AuBPs as well as their LSPR sensitivity.

# Chapter III. Gold nano-bipyramids as plasmonic enhancers in different bio-nano-sensor designs

## III.1 Introduction

One of the main goals of the bio-nano-technology research community is to develop and improve innovative nanoplatforms, which are able to sensitively and efficiently detect specific biomarkers in the incipient stages of the corresponding disease by highlighting the changes they sustain at the molecular level in the body [34]. The topic has attracted a lot of scientific attention since an early diagnostic could have a major impact on the patients' health enabling the implementation of an adequate treatment strategy – with less threatening side effects on healthy tissues/organs, and monitorization of the disease progression or regression.

## III.2 AuBPs-based immunosensor in solution for LSPR-SERS-SEIRA detection

In the following, we aim to develop a novel synergistic LSPR-SERS-SEIRA-active immunosensor in aqueous solution able to evidence specific antibody-antigen recognition interactions using gold bipyramids as plasmonic enhancers. The feasibility of the immunosensors as proven by employing the biotin-streptavidin interaction as "proof-of-concept". In order to validate our immunosensor design and sensing capabilities, the AuBPs performances were tested for the specific anti-human IgG- human IgG binding event. Hence, we demonstrated a reference design for dual-optical detection of target proteins in aqueous solution.

### III.2.1 Investigation of the SERS and LSPR sensitivity as function of the AuBPs' aspect ratios

The development of efficient LSPR-SERS nanoplatforms is based on the exploitation of the tunability of optical response of the AuBPs in combination with the amplified electromagnetic field present at their sharp tips. In order to evaluate the sensitivity for both SERS and LSPR sensing techniques, the p-aminothiophenol (p-ATP) molecule was further used as target molecule.

[34] Ibtisam Tothill and Zeynep Altintas, "Molecular Biosensors: Promising New Tools for Early Detection of Cancer," *Nanobiosensors in Disease Diagnosis*, January 2015, 1, https://doi.org/10.2147/NDD.S56772.

The identification of the characteristic Raman bands of the p-ATP molecule demonstrates that all AuBPs@p-ATP samples are SERS active. The SERS performance increases as the LSPR is localized closer to the excitation wavelength, as it distances itself from the 785 nm wavelength the efficiency of those AuBPs nanoplatforms decreases. Simultaneously, the LSPR sensing performance of the same AuBPs nano-systems was evaluated. The assessment is made based on the monitoring of the dependence of the *surface* RIS with respect to the LSPR band wavelengths. Similarly, as in SERS, all samples exhibit LSPR sensitivity by revealing red-shifts of the longitudinal LSPR peak, while the transversal contributions in the spectra remain stationary and unaffected, thus being in good agreement with the SERS results that the p-ATP molecules are located at the sharp ends of the nanostructures.

### III.2.2 Preparation of the Raman-labelled recognition element

A first step, when aiming to develop specific, sensitive, and efficient detection nanoplatforms, is to test their biosensing capabilities using a well-studied interaction such as the biotin-streptavidin antibody-antigen interaction as a "proof-of-concept".

Herein, we propose to chemically label the biotin molecule with the already studied p-ATP Raman reporter. In order to chemically from the p-ATP activated biotin (p-ATP@biotin) system, an adapted version of an already reported procedure was used [35]. Commercially available biotin-NHS and p-ATP solutions with the same concentration of 0.318 mmol were prepared. The p-ATP was added dropwise to the biotin-NHS solution under controlled conditions: nitrogen atmosphere and mild stirring. The final mixture was left under mild stirring overnight. The final product was obtained after the excess of reactants was removed by evaporation and precipitation. For further use, a solution of 15 mM p-ATP@biotin was prepared in $C_3H_8O$.

In order to confirm the coupling between the p-ATP and the biotin molecule, a spectroscopic characterization of the recognition element was pursued by employing the FT-IR spectroscopy. Additionally, the experimentally obtained spectroscopic results were compared with quantum chemical calculations in order to accurately assign the vibrational frequencies of the p-ATP and the p-ATP@biotin compounds. Concretely, the characteristic vibrational bands of the p-ATP and biotin are present in both experimental and simulated spectra of the chemically labelled p-ATP@biotin indicating their presence.

[35] Jiang et al., "Biotinylated Glyco-Functionalized Quantum Dots."

### III.2.3 Biosensing protocol

To the freshly purified AuBPs a p-ATP@Biotin solution is added, after a gentle stir, the mixture undergoes a thermal treatment in the drying stove at 45 ºC for 30 minutes, which favours the grafting of the newly prepared compound to graft to the gold surface. Following the heat treatment, the mixture is left undisturbed for 24 h at room temperature. To note, this system will further be denoted as p-ATP@Biotin-AuBPs. For the specific binding, the p-ATP@Biotin-AuBPs were incubated with the target protein. The final solution was left undisturbed overnight at room temperature.

### III.2.4 Multimodal LSPR-SERS-SEIRA detection – "proof-of-concept"

The biotin-streptavidin interaction is widely used in the development of biological assays due to its high specificity and strength of the bond thus being well-suited for the testing of the sensing nanoplatforms. Our proposed system takes advantage of this recognition interaction standing as "proof-of-concept" for the efficiency and sensitivity of the developed immunosensor.

In order to evidence the biotin-streptavidin interaction, the LSPR response of the p-ATP@Biotin-AuBPs was recorded using a UV-Vis-NIR spectrophotometer before and after the specific streptavidin capture as presented in Figure III.2.4.(a). Compared with the colloidal AuBPs, the p-ATP@Biotin-AuBPs present an 11nm red-shift of the longitudinal LSPR band confirming the successful grafting of the p-ATP activated biotin molecule. Once the streptavidin protein is captured by the biotinylated hybrid nanosystem, an additional 2 nm red-shift of the longitudinal LSPR is recorded (Figure III.2.4.(a)). These sensitive red-shifts confirm the specific detection of the protein.

Furthermore, we performed theoretical simulations using the FDTD method (using the commercially available FDTD solutionsTM software from Lumerical Inc. [36]), which well-reproduced the experimentally obtained results (Figure III.2.4.(a) – Inset on the right). Thus, both the experiment and theory confirm the successful and efficient detection of the recognition biotin-streptavidin interaction.

Complementary to the LSPR spectroscopy, an ultrasensitive technique for quantitative detection and analysis of target analyte at low concentration is represented by the Raman spectroscopy, for which the gold nanoparticles represent a real advantage due to their enhanced electromagnetic field (EM) localized at their surface. Subsequently,

[36] *Lumerical Www.Lumerical.Com/Products/*, n.d.

SERS spectra were recorded before and after the streptavidin capture to demonstrate the successful formation of the p-ATP@Biotin-AuBPs nanosystem (Figure III.2.4.(d)). The successful grafting of the p-ATP@Biotin chemically-labelled molecules was proven by the identification of the p-ATP characteristic bands [37] along with the characteristic vibrational bands of the free biotin molecule.

Once the streptavidin protein is captured by the biotinylated nanosystem, the SERS spectrum suffers a significant change as seen in Figure III.2.4.(d) – spectrum d. The identification of the major vibrational bands and their assignment is presented in Figure III.2.4.(e).

Furthermore, a quantitative analysis of the SERS performance was studied. Thus, an extended LOD of $10^{-12}$ M was obtained for the proposed immunosensor through the SERS detection. Similarly, the LSPR LOD was determined by monitoring the LSPR red-shift up to a streptavidin concentration of $10^{-7}$ M.

Similarly, to the SERS technique, SEIRA takes advantage of the enhanced local electromagnetic field arisen at the tips of the AuBPs allowing thus an increased infrared (IR) absorption by the AuBPs-attached molecules. Firstly, the successful coupling of the p-ATP@Biotin to the AuBPs surface was validated by recording the FT-IR spectra before and after the grafting process. The successful labelling of the biotin molecules with p-ATP is certified firstly through the appearance of the characteristic p-ATP vibrational modes found in both experimental and theoretical spectra of the p-ATP@Biotin sample along with the characteristic vibrational bands of the biotin molecule. Next, the specific biotin-streptavidin recognition interaction is confirmed by the presence of amide I and amide II bands in the FT-IR spectrum of p-ATP@biotin-AuBPs after bonding of streptavidin [38]. Respecting the same experimental conditions as for the LSPR and SERS evaluation, the LOD for the SEIRA detection was established to be $10^{-12}$ M.

[37] Baia et al., "Surface-Enhanced Raman Scattering and Density Functional Theoretical Study of Anthranil Adsorbed on Colloidal Silver Particles."
[38] M. J. Swamy, T. Heimburg, and D. Marsh, "Fourier-Transform Infrared Spectroscopic Studies on Avidin Secondary Structure and Complexation with Biotin and Biotin-Lipid Assemblies," *Biophysical Journal* 71, no. 2 (August 1, 1996): 840–47, https://doi.org/10.1016/S0006-3495(96)79285-8.

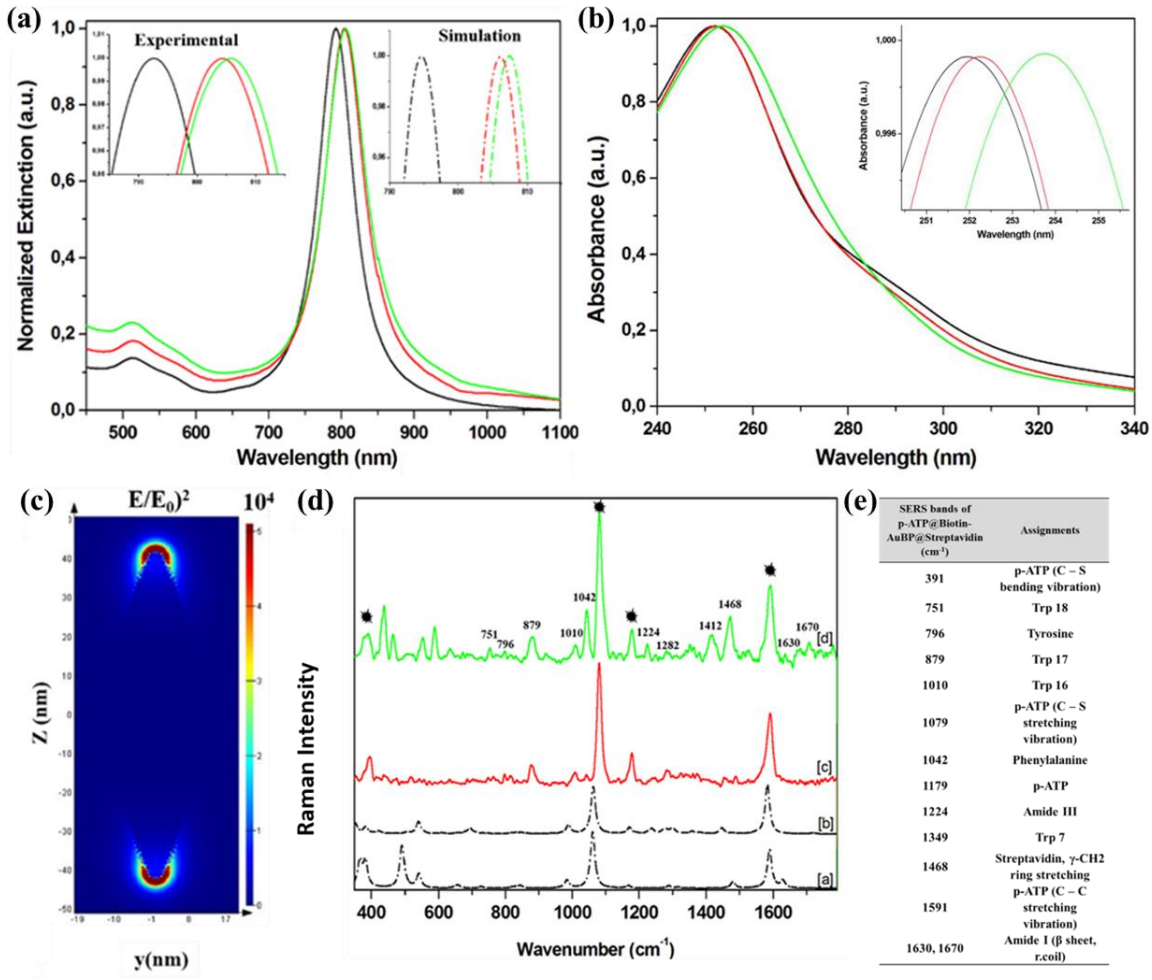


**Figure III.2.4. (a)** Extinction spectra recorded after each step of the biosensing protocol. Insets show the close-up of the experimental (solid spectra) and FDTD simulated extinction spectra obtained for the considered AuBPs (dotted spectra); **(b)** Absorption spectra of the p-ATP@Biotin (black spectrum), p-ATP@Biotin-AuBPs before (red spectrum) and after (green spectrum) the specific streptavidin detection; **(c)** Calculated $|E/Eo^2|$ map for the selected AuBPs exposed to the 785 excitation wavelength; **(d)** DFT simulated Raman spectra of p-ATP@Au (spectrum a) and p-ATP@Biotin-Au, respectively (spectrum b), along with the experimentally obtained SERS spectra of p-ATP@Biotin-AuBPs before (spectrum c) and after the capture of the streptavidin (spectrum d); **(e)** Assignment of the major SERS bands in the spectrum of biotin-streptavidin complex.

### III.2.5 Real sample application – detection of the human anti-IgG- human IgG immunological interaction

In order to further demonstrate the feasibility of the immunosensor for real clinical diagnostic applications, the colloidal AuBPs were implemented to highlight the specific

anti-human IgG- human IgG binding event [39]. Firstly, the optical response was monitored indicating that each step of the functionalization process induces successive LSPR red-shifts, thus the successful formation of the immunocomplex is confirmed validating the AuBPs as efficient and feasible LSPR nanosensors. Next, despite the fact that SERS is generally sensitive for the first layer of absorbed molecules [40], in the case of our AuBPs-based immunosensor the specific anti-human IgG – human IgG binding events has been detected due to the changes observed in the SERS fingerprint as a consequence of the recognition interaction. The variation of the bands, vibrations of the Phe residues, demonstrates the specific recognition interaction as it was also reported by Han et al., who has also concluded that the intensity ratio of these bands is dependent on the IgG concentration [41].

### III.2.6 Conclusions

To summarize, this study has aimed to develop a new multi-modal LSPR-SERS-SEIRA nanoplatform taking advantage of colloidal gold bipyramidal-shaped nanoparticles. The feasibility of the designed immunosensor was proven as a "proof-of-concept" by detecting the specific biotin-streptavidin interaction reaching LODs up to $10^{-12}$ M and, further, validated by its implementation in real sample applications such as the anti-human IgG-human IgG immunological interaction.

## III.3 Plasmonic paper-based nano-sensor for multimodal detection

In our study, we aim to respond to the demands by designing an innovative concept of a nanosensor directly on paper by employing an inexpensive calligraphy approach in order to test the LSPR-SERS-MEF detection of the specific biotin-streptavidin recognition interaction as a "proof-of-concept". The proposed fabrication method is inexpensive, easy to implement, rapid and much more suitable for spatial multiplexing [42]. Such a biosensing nanoplatform holds promising results for medical applications opening interesting routes for the development of innovative multiplex POC biochips.

[39] Zhuyuan Wang et al., "SERS-Activated Platforms for Immunoassay: Probes, Encoding Methods, and Applications," *Chemical Reviews* 117, no. 12 (June 28, 2017): 7910–63, https://doi.org/10.1021/acs.chemrev.7b00027.
[40] Kwan Kim, Hyoung Kun Park, and Nam Hoon Kim, "Silver-Particle-Based Surface-Enhanced Raman Scattering Spectroscopy for Biomolecular Sensing and Recognition," *Langmuir* 22, no. 7 (March 2006): 3421–27, https://doi.org/10.1021/la052912q.
[41] Xiao Xia Han et al., "Label-Free Indirect Immunoassay Using an Avidin-Induced Surface-Enhanced Raman Scattering Substrate," *Small* 7, no. 3 (February 7, 2011): 316–20, https://doi.org/10.1002/smll.201001936.
[42] Limei Tian et al., "Bioplasmonic Calligraphy for Multiplexed Label-Free Biodetection," *Biosensors and Bioelectronics* 59 (September 2014): 208–15, https://doi.org/10.1016/j.bios.2014.03.043.

### III.3.1 Fabrication of the paper-based nano-sensor through the plasmonic calligraphy approach

For the fabrication of the low-cost nano-sensor, a commercial Schneider ball-point pen and corresponding empty refillable cartridges were purchased from a local office supply store. Each cartridge was then filled with colloidal AuBPs. Spatially isolated lines were then drawn on the common Whatman No. 1 laboratory filter paper stripes. The obtained plasmonic paper-based substrates were allowed to dry at room temperature. The procedure was implemented three times, each draw was followed by a drying step.

### III.3.2 Characterisation of the as-designed plasmonic paper-based nanoplatform

The first step was to assess the optical properties of the as-fabricated nano-sensor by recording the extinction spectra of each plasmonic line (Figure III.3.2.- solid spectra). Hence, plasmonic paper-based nanoplatforms with tuneable LSPR responses were obtained: paper@AuBPs 618 with LSPR at 618 nm (black spectrum), paper@AuBPs 675 with LSPR at 675 (blue spectrum) and paper@AuBPs 800 with LSPR at 800 nm (green spectrum), respectively.

Herein, the AuBPs were intentionally fabricated to exhibit specific LSPR responses in order to achieve after the immobilization of the AuBPs onto the paper substrate longitudinal LSPR bands located in and out of resonance with the emission maximum of the streptavidin protein conjugated with Alexa 680.

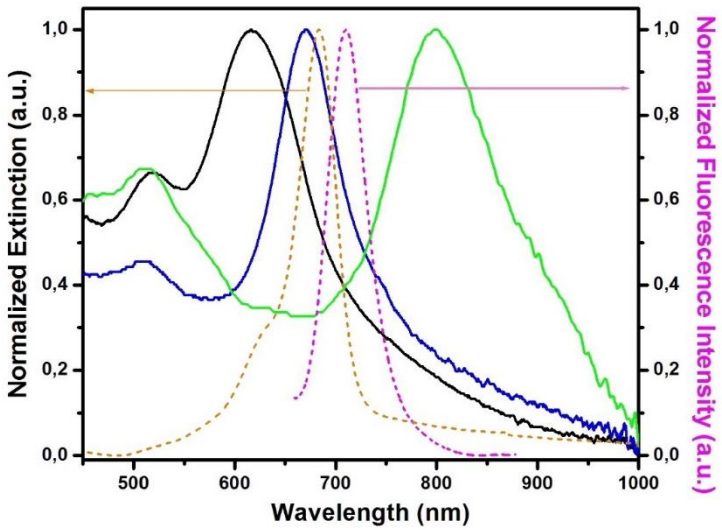


**Figure III.3.2.** The normalized extinction spectra of the plasmonic nanoplatforms (solid spectra) overlapped with the absorption (orange dashed spectrum) and fluorescence emission (magenta dashed spectrum) of the free streptavidin@Alexa 680 conjugate adsorbed on the bare Whatman paper.

Further, to understand the manner in which the nanoparticles attach to the paper substrate and specifically onto the cellulose fibres, the issue of the plasmonic nanoplatform's morphology was addressed. Consequently, the SEM technique was employed proving an individual distribution of the nanoparticles. HR-TEM images indicate that the AuBPs' shape and size was not damaged throughout and after the immobilization process. Furthermore, the HR-TEM technique also allows the visualization of the crystallographic planes of the nanostructures. Thus, the AuBPs bind to the cellulose fibres using their faces, leaving the highly sensitive tips of the nanostructures exposed for the easy access of target analytes grafting.

### III.3.3 Optimization of the plasmonic nanoplatform and sensitivity evaluation

In the development of plasmonic bio-detection devices, the optical efficiency plays a major role being determinant in the biosensing performances of the nanoplatform. Subsequently, a strategy to enlarge the AuBPs loading onto the paper cellulose strands and, thus, increase the optical density was developed. The strategy consists in the repetition of the proposed plasmonic calligraphy approach and monitoring the longitudinal LSPR band intensities. The optical density reaches a saturation plateau after 5 to 6 repetitions for all three tested nanoplatforms. Further, the nanoplatforms were placed in different environments to evaluate their biosensing capabilities. *bulk* RIS values from 83 nm/RIU to 287 nm/RIU were determined.

### III.3.4 Biosensing protocol

The proposed biosensing protocol implies the successive addition of 1.5 mM p-ATP@Biotin and 0.25 mg/ml Streptavidin@Alexa 680 (in PBS pH 7.2) on the plasmonic lines drawn on the paper substrate. The target Streptavidin@Alexa 680 molecule was chosen to promote MEF, thus the p-ATP@Biotin@Streptavidin become not only indicators of the recognition interaction detection but also the needed spacer to ensure a convenient distance between the gold surface and fluorophore for MEF to occur hence extending the detection capabilities of the developed nano-sensor.

### III.3.5 Multimodal LSPR-SERS-MEF detection

The functionalization with the p-ATP activated biotin was confirmed through UV-Vis-NIR spectroscopy for all three designed paper-based nanoplatforms by recording the extinction spectra before (red spectra) and after (green spectra) the grafting procedure (Figure III.3.5.(a-c)).The change of the RI of the environment in the close vicinity of the

nanostructures arsen as a consequence of the p-ATP@Biotin binding induces red-shifts of the longitudinal LSPR bands of all plasmonic nanoplatforms ranging from 13 to 17 nm. However, the specific identification of the p-ATP activated biotin molecule is realized through SERS measurements. The SERS technique is more sensitive and allows the differentiation of the Raman fingerprint of the molecule of interest. Figures III.3.5.(d-f) show comparative SERS spectra of the biotinylated plasmonic lines confirming the successful functionalization process by identifying, firstly, the characteristic vibrational bands of the p-ATP Raman reporter and, secondly, the unique Raman signature of the biotin molecule [43].

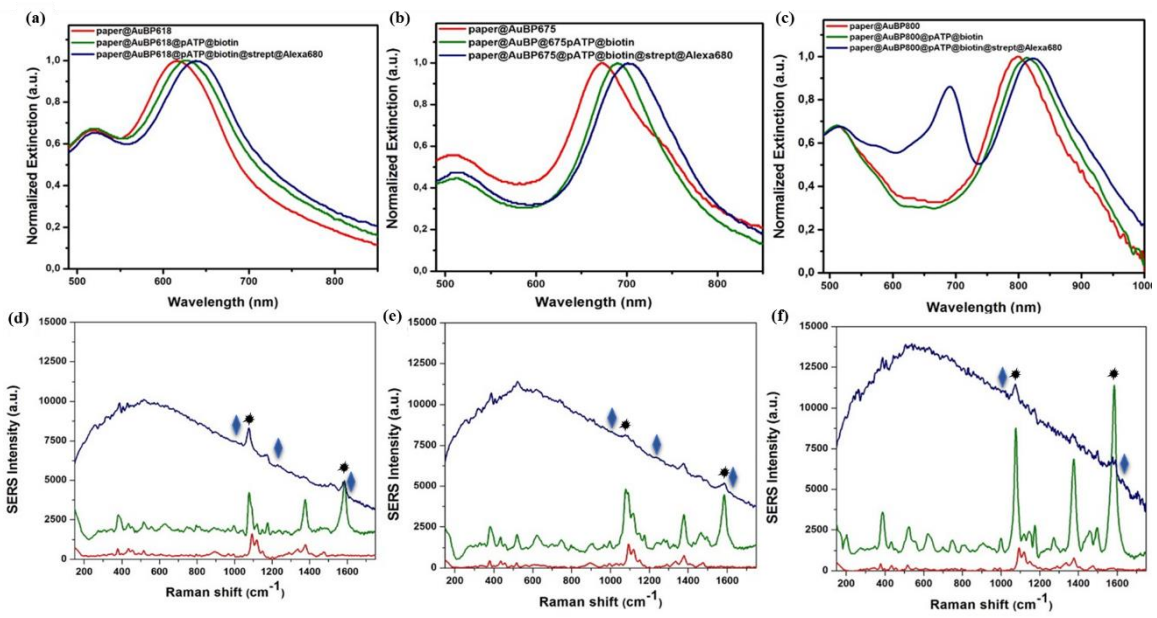


**Figure III.3.5.** Normalized extinction spectra **(a-c)** together with the recorded SERS spectra **(d-f)** of the as-designed paper-based plasmonic nanoplatforms with tuneable plasmonic response before (red spectra), after their biotinylating process (green spectra), and after the specific capture of target streptavidin (blue spectra), proving the capability of our nanoplatforms for dual LSPR-SERS detection.

Further, after the successful capture of the protein by the p-ATP@Biotin functionalized paper-based plasmonic nanoplatforms, the LSPR bands exhibit an additional 14 to 18 nm red-shifts (Figure III.3.5.(a-c) -blue spectra), which confirm the specific detection of the streptavidin and, thus, the successful antibody-antigen recognition

[43] Galarreta, Norton, and Lagugné-Labarthet, "SERS Detection of Streptavidin/Biotin Monolayer Assemblies †";
Andreea Campu et al., "Gold NanoBipyramids Performing as Highly Sensitive Dual-Modal Optical Immunosensors," *Analytical Chemistry* 90, no. 14 (July 17, 2018): 8567–75, https://doi.org/10.1021/acs.analchem.8b01689.

interaction. Next, the LSPR sensitivity was experimentally evaluated for the selected paper@AuBP 675 by the determination of a LOD of 0.01 mg/ml.

Additionally, the corresponding SERS spectra recorded after the specific biotin-streptavidin interaction (Figure III.3.5.(d-f) -blue spectra) clearly demonstrate the successful capture of the streptavidin@Alexa 680 complex. In addition to the dominant fluorescence signal from the Alexa 680 fluorophore, the characteristic Raman bands of the p-ATP are present along with the vibrational modes of the detected streptavidin protein. Furthermore, a more intense fluorescence emission signal is observed in the case of the paper@AuBPs 800 nanoplatform caused by the resonant excitation of the longitudinal LSPR band located at 800 nm, thus indicating the potential opportunity to detect SERS and MEF signals simultaneously.

At last, the effective MEF performance of the proposed paper-based plasmonic nanoplatforms was analysed. The fluorescence emission of the fluorophore was recorded both when the streptavidin@Alexa 680 complex was captured by the biotinylated plasmonic lines and when added to the bare Whatman filter paper near the plasmonic lines. The streptavidin@Alexa 680 on paper@AuBPs 675 reveals a 2-fold fluorescence emission enhancement when a 675 nm excitation wavelength was employed.

### III.3.6 Conclusion

To conclude, we designed an innovative flexible and tuneable plasmonic paper-based nanoplatform by calligraphing, using a commercial pen filled with AuBPs as plasmonic ink, different active plasmonic lines with modulated LSPR responses. The biotin-streptavidin recognition interaction was used as a “proof-of-concept” to demonstrate the potential of our designed plasmonic paper-based nanoplatform to be implemented as efficient biosensing device with multiplex LSPR-SERS-MEF capabilities. Thus, in the context of the importance of the development of miniaturized POC diagnostic devices, our inexpensive calligraphed paper-based plasmonic nanoplatform could be an excellent candidate of choice for further application in the multimodal detection of relevant biomarkers.

## III.4 Microfluidic channel integrated plasmonic bio-nano-sensor for detection in laminal flow

In this work, we develop a novel approach to design a robust low-cost microfluidic device which successfully integrates the efficiency of the AuBPs plasmonic enhancers allowing portability, reduced analysis time through dynamic measurements and high sensitivity. The proven features of our miniaturized portable plasmonic microfluidic system allowing the detection and identification of target analytes in laminal flow with high specificity, accuracy and efficiency represent the groundwork for further development in view of complex biosensing applications.

### III.4.1 Preparation of the plasmonic substrate

The cleaning process of commercially available glass slides was performed as follows: first, the glass slides were washed with chromic mixture, ultrapure water and alkaline detergent, after they dried out at room temperature, a 30 minutes UV treatment at 25 ºC was applied using the PSD Pro Series Digital UV Ozone System.The silanization protocol implies the immersion of the clean glass substrates in a 10% APTES (in ethanol) solution for 1 hour [44]. The proposed nanoparticle deposition strategy consists of the drop-wise addition of the AuBPs on the silanized glass substrates being left overnight at room temperature to attach to the functionalized substrate.

### III.4.2 Optical and morphological characterisation of the plasmonic substrate

The first step after the deposition of the AuBPs onto the silanized glass substrate, was to investigate the morphology of the glass@AuBPs using the SEM and employ the UV-Vis-NIR spectroscopy to investigate its optical properties. Representative SEM microscopic images were recorded at two magnifications, which indicate a homogeneous coverage of the AuBPs on the surface of the glass substrate. Additionally, it is observed that the AuBPs have attached in two different arrangements: as individual nanoparticles with well-defined shape and self-assembled in an end-to-end manner as short AuBPs chains. The morphological observations are sustained by the spectroscopic investigations as three bands are distinguished in the extinction spectra of the glass@AuBPs: a band located at 515 nm assigned to the transversal optical response, a narrow band at 685 nm associated with the longitudinal LSPR response of the AuBPs and a new band at 825 nm

[44] Seunghyun Lee, Kathryn M. Mayer, and Jason H. Hafner, "Improved Localized Surface Plasmon Resonance Immunoassay with Gold Bipyramid Substrates," *Analytical Chemistry* 81, no. 11 (June 1, 2009): 4450–55, https://doi.org/10.1021/ac900276n.

arisen due to the plasmon coupling between the AuBPs indicating the end-to-end formation of self-assemblies confirmed also through numerical simulations.

### III.4.3 *Bulk* refractive index sensitivity of the plasmonic substrate

In order to assess the LSPR detection capabilities, the *bulk* RIS of the glass@AuBPs was determined by exposing the functionalized glass substrate to different RI environments. The increasing RI induces strong red-shifts of the longitudinal LSPR response as well as of the new band assigned to the AuBPs formed chains. After performing a linear regression, RIS values of 243 nm/RIU and a coefficient of determination ($R^2$) of 0.997 for the individual AuBPs and 150 nm/RIU for the plasmon coupling were determined.

### III.4.4 Fabrication of the microfluidic channels and integration of the plasmonic substrate

For the fabrication of the microfluidic channels, the replica moulding technique was used as it has been developed and reported by our group [45]. Onto the mould, a 10:1 mixture of the optically transparent PDMS elastomer and its curing agent – as cross-linking agent, was poured after being degassed for 30 minutes. The obtained system underwent a thermal treatment at 65 ºC for 1 h. Finally, the microfluidic channels were peeled of the mould. The next step was to integrate the previously fabricated plasmonic substrate into the microfluidic channel, therefore, both elements were plasma treated. Immediately after the curing process, they were brought into contact thus creating a permanent bond [46].

### III.4.5 Dual-modal LSPR/SERS detection in laminal flow

The LSPR-SERS detection efficiency in laminal flow of our as-designed integrated plasmonic microfluidic device was assessed by employing the well-known Raman reporter p-ATP [47] and a portable Raman system with 785 nm excitation wavelength. For the validation of the LSPR-SERS detection capabilities, a p-ATP solution of $10^{-6}$ M was

[45] Monica Iosin et al., "Laser Microstructuration of Three-Dimensional Enzyme Reactors in Microfluidic Channels," *Microfluidics and Nanofluidics* 10, no. 3 (March 1, 2011): 685–90, https://doi.org/10.1007/s10404-010-0698-9;
Monica Focsan et al., "Two-Photon Fabrication of Three-Dimensional Silver Microstructures in Microfluidic Channels for Volumetric Surface-Enhanced Raman Scattering Detection," *Optical Materials Express* 6, no. 5 (May 1, 2016): 1587–93, https://doi.org/10.1364/OME.6.001587.
[46] Alex Y. N. Hui et al., "Microwave Plasma Treatment of Polymer Surface for Irreversible Sealing of Microfluidic Devices," *Lab on a Chip* 5, no. 10 (October 2005): 1173–77, https://doi.org/10.1039/b504271b;
Liangcai Xiong, Peng Chen, and Quansheng Zhou, "Adhesion Promotion between PDMS and Glass by Oxygen Plasma Pre-Treatment," *Journal of Adhesion Science and Technology* 28, no. 11 (June 3, 2014): 1046–54, https://doi.org/10.1080/01694243.2014.883774.
[47] M. Baia et al., "Probing the Enhancement Mechanisms of SERS with P-Aminothiophenol Molecules Adsorbed on Self-Assembled Gold Colloidal Nanoparticles," *Chemical Physics Letters* 422, no. 1–3 (April 2006): 127–32, https://doi.org/10.1016/j.cplett.2006.02.054.

prepared and injected into the microchannel. As the laminal flow of the p-ATP was started, first the LSPR detection was addressed by recording the LSPR spectrum. Compared to the glass@AuBPs optical response, the longitudinal LSPR band exhibits an 18 nm red-shift along with a 9 nm red-shift of the band assigned to the plasmon coupling confirming the detection of the p-ATP analyte. Furthermore, the specific identification of the molecule is ensured by the SERS investigation of the same spot. The Raman spectrum of the solid p-ATP is compared to the SERS spectrum acquired in laminal flow, both exhibiting the characteristic vibrational bands of the Raman reporter. Thus, we confirmed that the p-ATP molecules graft covalently at the tips of the nanostructures as well as in the interparticle gaps formed by the linked AuBPs.

Furthermore, the SERS performance of the plasmonic integrated microfluidic device was evaluated by the determination of its LOD. The extracted intensities were then plotted against the p-ATP concentrations and fitted using an exponential model with a regression coefficient $R^2$ of 0.994. Thus, a LOD as low as $10^{-14}$ M was determined using the SERS technique, proving the high sensitivity of the designed microfluidic device.

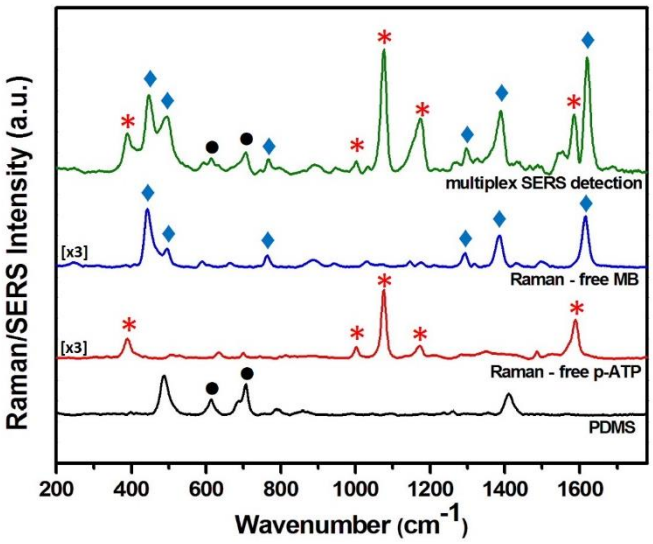


**Figure III.4.5.** Raman spectra of PDMS (black spectrum), free p-ATP (red spectrum) and Methley blue (blue spectrum) together with SERS spectrum of multiplex analytes inside the as-designed plasmonic device.

Taking into consideration all the detection capabilities exhibited by our integrated plasmonic microfluidic device, its applicability was extended to multiplexed on chip SERS detection of two target analytes, specifically p-ATP and Methylene Blue (MB). Figure III.4.5. shows the Raman spectra obtained on the solid p-ATP and MB in comparison to

the SERS spectra recorded inside the microfluidic chip after both solutions were employed. Thus, the simultaneous presence of multiple SERS analyte signatures was validated by distinguishing two molecules grafted concomitantly on the gold surface.

### III.4.6 Conclusion

To summarize, this study reports an innovative approach to design and fabricate a miniaturized and portable microfluidic device with integrated plasmonic transducers enabling the rapid analysis to small volume samples. The AuBPs -as highly efficient nano-antennas, were deposited on the silanized glass substrate and further integrated into the PDMS microfluidic channel allowing thus the "online" detection and identification of the p-ATP molecule in laminal flow. The proposed design was proven to be highly efficient for both on-chip LSPR and SERS detection techniques. Furthermore, a LOD of $10^{-14}$ M was achieved by SERS as well as the identification of two analytes of interest simultaneously attached to the gold surface thus promoting multiplexed SERS detection capabilities. The high sensitivity of the detection and identification of target analytes in laminal flow of our portable miniaturized integrated plasmonic microfluidic device advocate for its implementation in further complex biosensing applications.

# Chapter IV. Therapeutic applications of gold bipyramids

## IV.1 Introduction

Gold nanoparticles have gathered a lot of attention in the recent years as potential therapeutic agents, the concern is justified by their unique optical properties, specifically, the LSPR, which can be tuned to one's desire taking advantage of its dependency on the shape and size of the nanostructures. Specifically, nanostructures with absorption bands located in the NIR region are of interest for two main reasons: (i) in the NIR the tissues are optically transparent ensuring a higher penetration depth and (ii) the nanoparticles present better absorption/scattering features. AuBPs exhibit attractive optical properties by allowing the fine tuning of their LSPR along the electromagnetic spectrum as well as presenting intrinsic non-radiative properties, thus conveying their suitability for therapeutic PTT-PDT applications.

## IV.2 Intrinsic therapeutic properties

In recent years, the AuBPs optical properties were intensively exploited and implemented in therapeutic nano-systems, which were, subsequently, validated as powerful plasmonic-based therapeutic agents [48]. In order to use these properties into our advantage, it is imperative to understand them at their fundamental principle. To reach such deep knowledge, a rigorous characterization of the AuBPs in terms of photothermal and photodynamic capabilities is highly desired, which to our best knowledge, at the time being, lacks from the specialty literature.

### IV.2.1 Photothermal properties and conversion efficiencies

The aim of this study is to determine the intrinsic photothermal abilities of the AuBPs, therefore, a meticulous analysis and evaluation of the photothermal properties of the as-synthesised AuBPs exhibiting different aspect ratios was realized.

The well-characterized AuBPs colloidal solutions were irradiated with the 785 and 808 nm excitation wavelengths for 30 minutes. Thermographic images were recorded during the irradiation and the reached temperatures ($T$) were extracted. In order to

[48] Jie Feng et al., "Bioconjugation of Gold Nanobipyramids for SERS Detection and Targeted Photothermal Therapy in Breast Cancer," *ACS Biomaterials Science & Engineering* 3, no. 4 (April 10, 2017): 608–18, https://doi.org/10.1021/acsbiomaterials.7b00021;
Jung-Hoon Lee et al., "Plasmonic Photothermal Gold Bipyramid Nanoreactors for Ultrafast Real-Time Bioassays," *Journal of the American Chemical Society* 139, no. 24 (June 21, 2017): 8054–57, https://doi.org/10.1021/jacs.7b01779;
Shuang Zhao et al., "High and Low Molecular Weight Hyaluronic Acid-Coated Gold Nanobipyramids for Photothermal Therapy," *RSC Advances* 8, no. 16 (2018): 9023–30, https://doi.org/10.1039/C7RA11667E.

determine the thermal contribution of the AuBPs, from the expressed $T$, the environmental temperature ($T_{env}$) was subtracted. The temperature difference ($\Delta T$) was then plotted as a function of time. Figure IV.2.1.(a) and (c) present the heat generation curves obtained after the exponential fit of the experimental data based on the theoretical model described by the energy balance equation. All samples attain the saturation plateau in a time interval from 14 to 15 minutes for both irradiation sources. In the case of the 785 nm laser line, $\Delta T$ varies from 5 to 18°C (Figure IV.2.1.(a)), while, for the 808 nm excitation wavelength, $\Delta T$ spans from 4 to 25°C.

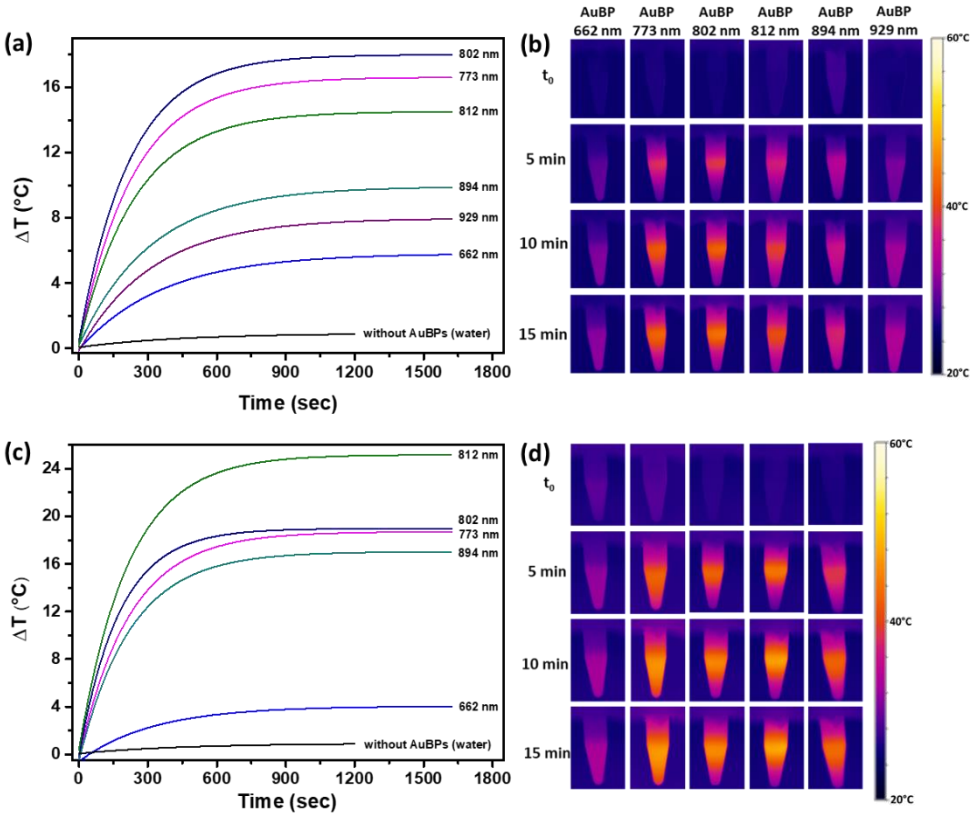


**Figure IV.2.1.** The fitted thermal plots of the AuBPs under irradiation with 785 **(a)** and 808 nm **(c)** excitation wavelengths and their corresponding thermographic images in time **(b)** and **(d)**.

Additionally, the obtained thermal curves are well-supported by the recorded thermographic images (Figure IV.2.1.(b) and (d)), the same determinations are made based on the thermographic maps following the arbitrary colour scale. The AuBPs 802 perform best when excited with the 785 nm laser line, while AuBPs 812 convert better light-to-heat at 808 nm irradiation wavelength.

Following the irradiation of the system, the AuBPs systems were investigated by employing 4 laser on/off cycles proving that the AuBPs samples reach the already defined $T_{max}$, thus demonstrating the high reproducibility of the previously obtained results. The optical response is well-reproduced even after 24 hours, thus confirming their high stability succeeding their thermo-plasmonic implementation.

The light-to-heat conversion potential of the nanostructures in general is assessed by the determination of the photothermal conversion efficiency (η). The calculated photothermal conversion efficiencies vary from 40% to 97%. Specifically, the AuBPs with LSPR at 802 nm express a η of 97% when irradiated with the 785 nm laser line, as in the case of the 808 nm excitation, the AuBPs with optical response at 812 nm perform best reaching a η of 74 %.

In the interest of optimising the experimental conditions, the thermal behaviour was monitored when parameters such as optical density, sample volume and laser power were varied one at a time. The heat generation process is faster when the nanoparticle' solution is more concentrated. The acceleration of the photothermal conversion mechanism is observed for the low sample's volumes. Moreover, an increase of the laser power generates an increase of the temperature.

In addition to the thorough optical and thermo-plasmonic characterization, the AuBPs underwent stability tests in biologically relevant experimental conditions thus validating them as promising therapeutic tools as response to the demands of the bio-nano-medicine research community.

### IV.2.2 Oxygen singlet generation

In order to have a better understanding of the therapeutic effect of the proposed AuBPs-based nano-system, the intrinsic photodynamic properties of the nanostructures were studied. Specifically, their ability to transfer electrons to the surrounding environment while under exposure to an external excitation source, aiming to induce photo-chemical reactions such as the generation of toxic ROS, i.e. $^1O_2$ – which is formed as a result of electron transfer from a photo-excited donors to the ground state oxygen [49]. From the recorded extinction spectra, the absorbances of the band located at 380 nm were extracted and fitted as plots of the ABDA amount in function of time. Thus, under the 785 nm excitation wavelength, the most efficient AuBPs are the ones presenting the LSPR response

[49] Reinhard Schmidt, "Photosensitized Generation of Singlet Oxygen," *Photochemistry and Photobiology* 82, no. 5 (April 30, 2007): 1161–77, https://doi.org/10.1562/2006-03-03-lR-833.

at 804 nm and expressing a 30% decrease of the ABDA amount, while, in the case of the 808 nm laser line, the nanostructures with the longitudinal optical response located at 815 nm decrease the ABDA amount with 32%, being the best from the investigated sample batch. Hence, these gold nanostructures prove themselves to be efficient PDT agents allowing the triggered release of ROS when submitted to a specific light excitation.

### IV.2.3 Conclusion

In summary, this work systematically analyses intrinsic photothermal and photodynamic properties of the gold nano-bipyramids with different aspect ratios upon the exposure to two NIR laser sources. Considering their strong optical absorption all systems present a light-to-heat conversion ability, however, the most efficient AuBPs with regard to the laser lines employed are: AuBPs@802 under 785 nm irradiation and AuBPs@812 under 808 nm exposure presenting photothermal conversion efficiencies of $\eta_{802}$ = 97% and $\eta_{812}$ = 74%, respectively. Furthermore, as this effect is less investigated in literature, the photodynamic activity of AuBPs was measured by monitoring the photooxidation of ABDA, counting for a 30% decrease in ABDA optical absorbance for the most active AuBPs, which well-correlates with the previously determined light-to-heat photothermal conversion efficiency.

## IV.3 ICG-loaded gold nano-bipyramids with NIR activatable dual PTT-PDT therapeutic potential in melanoma cells

This work aims to integrate the therapeutic activities of two NIR photoactive biomaterials into a one single targeted hybrid nanosystem able to operate as dual PTT - PDT agent with higher efficiency compared with each one alone. An AuBPs-based nano-system was designed and validated for the dual PTT-PDT therapy in solution as well as *in vitro* using B16-F10 melanoma cells.

### IV.3.1 Bio-compatibilization and ICG-loading protocols

In order to improve the biocompatibility of the as-fabricated AuBPs, a 1% PLA stock solution was prepared by dilution in $CH_2Cl_2$, which was then added to the colloidal AuBPs in an AuBPs:PLA=1:10 volume ratio. As the phase separation process is complete, the AuBPs@PLA are recovered. The coating of the AuBPs with the PLA biopolymer was confirmed by UV-Vis-NIR spectroscopy as the longitudinal LSPR band of the nanostructures is blue-shifted with respect to the as-prepared AuBPs with 8 nm. Moreover,

the hydrodynamic diameter of the AuBPs before and after the grafting process was confirmed also by DLS measurements.

Next, our aim is to enhance the intrinsic therapeutic performances by grafting/loading the ICG molecule onto the AuBPs surface. The ICG dye is known to exhibit both photothermal and photodynamic properties, hence it can supplementary amplify the PTT-PDT therapeutic activity of the plasmonic nanosystem. For the grafting, a 1 mg/ml ICG methanolic stock solution was added to the AuBPs@PLA solution leading to a loading efficiency of 41 %. The efficient binding of the ICG on the AuBP@PLA hybrid systems was evidenced by absorption spectroscopy.

### IV.3.2 Photothermal and photodynamic properties in Solution

Following the design of the AuBPs@PLA@ICG system, its photothermal and photodynamic properties were investigated and compared with the intrinsic properties of the AuBPs (Figure IV.3.2.). In the case of the AuBPs (black plot) the temperature of the environment is increased by 17°C, whereas, after the grafting of the ICG molecules, the AuBPs@PLA@ICG (red plot) heats up the medium with an additional 2°C given the dyes' capability to be photothermally active and supplementary contribute to the overall PTT performance. The obtained nanosystem reaches a slightly variable $T_{max}$ thus proving the high thermal stability of the AuBPs@LA@ICG nanoplatform.

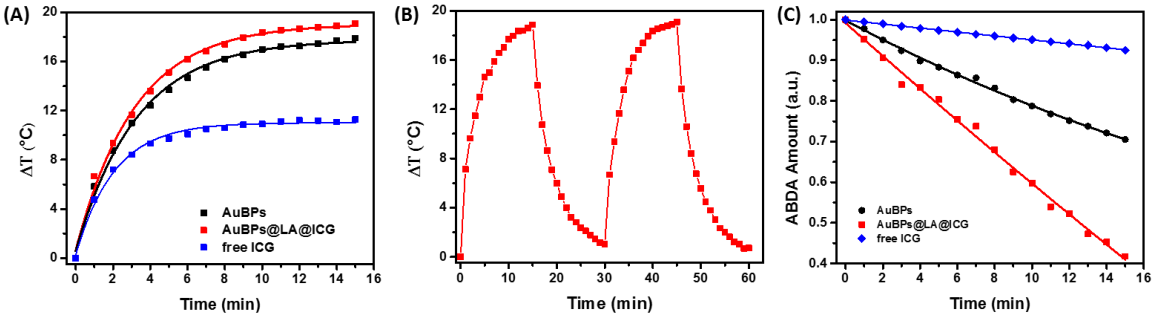


**Figure IV.3.2. (a)** The thermal curves obtained after the exponential fit of the temperature variations, **(b)** the thermal curves of AuBPs@PLA@ICG after two ON-OFF irradiation cycles and **(c)** the fitted plots of the ABDA amount decrease with respect to the employed photodynamic system.

Similarly, the $^1O_2$ generation capabilities of the nanosystem were compared with the intrinsic photodynamic features of the AuBPs (Figure IV.3.2.(c)). The AuBPs@PLA@ICG (red plot) decreases the ABDA amount with 60%, which suggests that

the ICG is responsible for doubling the photodynamic activity of the free AuBPs (black plot). Additionally, the photothermal conversion efficiencies (η) and the oxygen singlet quantum yields ($\Phi(\,^1O_2)$) were determined. The cumulated effects of the final hybrid nanosystem lead to a 76 % efficiency to convert light-to-heat, while a $^1O_2$ quantum yield of 0.297 was determined for the 785 nm excitation wavelength.

### IV.3.3 Targeting functionalization and validation of the in vitro dual PTT – PDT therapy

The aim of this study is to assess the nanoparticles' capabilities to act as efficient therapeutic agents for cancer treatment, in vitro studies were performed on melanoma cells (B16-F10). The targeting functionality of the AuBPs@PLA@ICG is ensured by the conjugation with activated NHS-EDC FA. The B16-F10 cell line overexpresses the folate receptor at their membrane, thus capturing the FA present at the surface of the hybrid nanoparticle-based system. Lately, folate receptors are considered to be selective drug targets for the treatment of cancer and currently are included in different target therapies. It is known that folate receptors are overexpressed in malignant tissues of epithelial origin compared to normal ones [50]. The presence of folate-receptor in human and mouse melanoma cell lines in primary and metastatic tumors from melanoma patients was confirmed. Recently, it was reported that the staining for the folate receptor of B16-F10 gives a strong signal in the confocal microscopy analysis [51].

First, the AuBPs were functionalized with the EDC-NHS activated folic acid cellular recognition element [52] for further use in in vivo experiments. After the conjugation with the activated FA, the recorded longitudinal LSPR band of the AuBPs presents an additional 4 nm red-shift confirming thus the successful functionalization process.

The biocompatibility was checked using a the WST-1 assay. The AuBPs proved to be straight-forward toxic in concentrations higher than 63μM, whereas, after being successively covered with the biocompatible PLA, ICG and FA, the nano-systems have improved the inhibition concentration (IC50) limit to 84 μM. Due to the AuBPs property

[50] Luís Sánchez-del-Campo et al., "The Critical Role of Alpha-Folate Receptor in the Resistance of Melanoma to Methotrexate," *Pigment Cell & Melanoma Research* 22, no. 5 (October 2009): 588–600, https://doi.org/10.1111/j.1755-148X.2009.00586.x.
[51] Y. Chen et al., "Overcoming Multidrug Resistance Using Folate Receptor-Targeted and PH-Responsive Polymeric Nanogels Containing Covalently Entrapped Doxorubicin," *Nanoscale* 9, no. 29 (2017): 10404–19, https://doi.org/10.1039/C7NR03592F.
[52] Ronak H. Patel et al., "Multifunctionality of Indocyanine Green-Loaded Biodegradable Nanoparticles for Enhanced Optical Imaging and Hyperthermia Intervention of Cancer," *Journal of Biomedical Optics* 17, no. 4 (April 2012): 046003, https://doi.org/10.1117/1.JBO.17.4.046003.

to efficiently scatter light, the internalization of the nano-system was evidenced by dark-field microscopy (Figure IV.3.3.(a) and (b)).

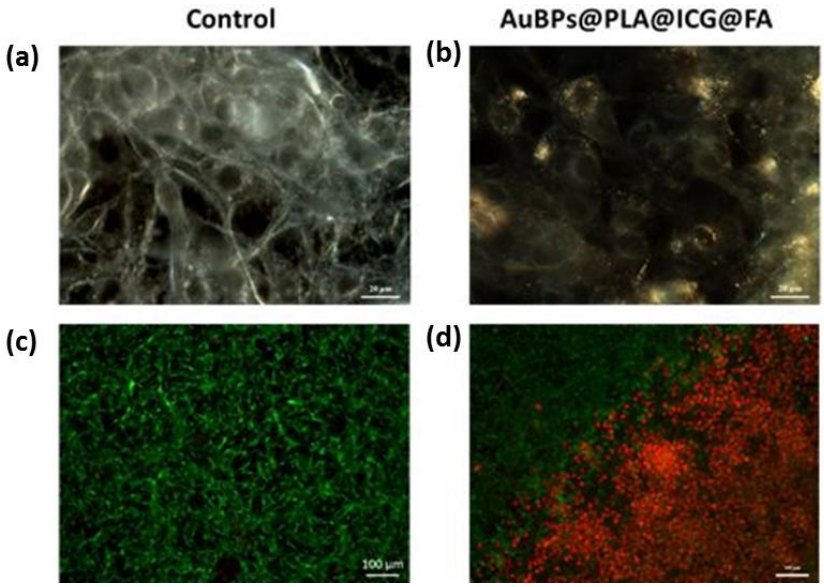


**Figure IV.3.3. (a),(b)** Dark field microscopy images of the control and AuBPs@PLA@ICG@FA treated cells before irradiation and **(c),(d)** fluorescence microscopy images of the control and AuBPs@PLA@ICG@FA after the irradiation and staining with CA (green) and PI (red).

Further, to visualize the therapeutic effects after the irradiation, the non-treated (control) and AuBPs@PLA@ICG@FA treated B16-F10 cells were stained with fluorescent dyes: calcein (CA – green color), to stain the living cells, and propidium iodide (PI – red color), for the dead cells. Figure IV.3.3.(c) shows the irradiated untreated control B16-F10 cells, indicating that laser exposure had little antitumor efficacy, displaying the unaffected green coloured living cells. In contrast, in the situation of the B16-F10 cells exposed to 42 µM AuBPs@PLA@ICG@FA treatment for 24h and then irradiated, the laser proved to have a massive antitumor efficacy presented to be more than 90%, as can be seen in Figure IV.3.3.(d), as red stained cells in right-bottom of the image.

### IV.3.4 Conclusions

To summarize, our work proposes the design of an efficient AuBPs-based dual photothermal-photodynamic hybrid nanoplatform with improved PTT-PDT performances. The most efficient AuBPs, in terms of intrinsic PTT and PDT activity, were coated with PLA, which ensures both biocompatibility as well as the biopolymeric matrix for ICG grafting. The NIR dye photothermal and photodynamic activities enhance the overall PTT-PDT efficiency by rising the temperature with 2°C and doubling the $^1O_2$ species generation.

Following the bioconjugation with FA, the internalization of the as-designed nano-system was ensured by the B16-F10 cells and successfully validated as dual PTT-PDT therapeutic agents presenting valuable results, which contribute to the improvement of the cancer treatment strategies based on smart nano-systems for clinical applications.

# Chapter V. Final Conclusions and Future Perspectives

## V.1 Final Conclusions

This work aimed to investigate and determine the feasibility of gold nano-bipyramidal nanoparticles (AuBPs) to be successfully integrated in the development of hybrid nanosystems with enhanced features which encourage their implementation in various medically relevant applications.

In this context, the main conclusions to bear in mind are the following:

- We have succeeded to synthesise highly reproductible AuBPs colloidal nanoparticles with tuneable longitudinal LSPR over the entire electromagnetic spectrum spanning from 600 to 1200 nm proving narrow LSPR, high RIS and FOM values, high homogeneity in size and shape and accessible surface chemistry.
- We have successfully chemically labelled the biotin molecules with the p-Aminothiophenol well-known Raman reporter and, thus, provided a biotinylated complex which was proven to play different vital roles, specifically: i) recognition element, ii) Raman label, iii) linker to the gold surface, and iv) spacer for MEF.
- The LSPR and SERS sensitivities of the AuBPs with different aspect ratios were investigated using the p-ATP target analyte, thus demonstrating that the AuBPs with LSPR at 793 nm are to be the most efficient with regard to the used experimental setup.
- The multimodal LSPR-SERS-SEIRA detection capabilities of the AuBPs in aqueous solution were demonstrated first by employing the biotin-streptavidin recognition interaction as “proof-of-concept”. The limits of detection were determined reaching $10^{-7}$ M for LSPR and $10^{-12}$ M for SERS and SEIRA sensing. The human IgG-anti IgG recognition interaction was successfully evidenced by dual LSPR-SERS detection.
- A new paper-based plasmonic nanoplatform was designed by employing an innovative deposition method, namely the calligraphy approach. This design was proven to enable multiplexing capabilities due to the fabrication of isolated plasmonic line domains. Along with the LSPR and SERS successful detection and identification of the elements involved in the biological event, the MEF detection was enabled proving a 2.05-fold enhancement of the Alexa 680 fluorescence emission.
- We have successfully integrated the AuBPs by their immobilization onto a functionalized glass substrate into a microfluidic device for the dual LSPR-SERS detection

of target analytes in laminal flow. The SERS LOD of $10^{-14}$ M was reached and the multiplexing capabilities were proven by the simultaneous identification of two analytes.

- The intrinsic photothermal properties of AuBPs with different aspect ratios were demonstrated by their photoexcitation with two NIR laser lines (i.e. 785 and 808 nm), thus determining photothermal conversion efficiencies ranging from 40 to 97 %.
- The AuBPs were proven to exhibit an intrinsic photodynamic activity by the monitoring of a scavenger molecule (i.e. ABDA) absorbance throughout their irradiation with the two NIR laser sources, counting for a 30 % ABDA reduction for the most active AuBPs. Thus, we have demonstrated their potential as PDT Therapeutic agents.
- We have succeeded to functionalize the most PTT and PDT efficient with polylactic acid, thus increasing their biocompatibility and enabling the incorporation of the Indocyanine Green (ICG) photosensitizer into the biopolymeric matrix.
- The simultaneous photoexcitation of both AuBPs and ICG has resulted into an increase of the PTT performance by 4 %, while the singlet oxygen quantum yield was determined to be 0.3. Thus, we have demonstrated the ability of the AuBPs to efficiently amplify the PTT and PDT performance of the ICG.
- The final system was successfully validated by the evaluation of the simultaneous dual PTT-PDT therapy in epithelial melanoma cells by employing the fluorescence microscopy.

All the obtained results encourage and support the utilization of the AuBPs for the development of innovative efficient, inexpensive, rapid, portable and miniaturized sensing devices as well as their implementation in therapeutic systems' designs for targeted and localized effective minimum invasive PTT-PDT therapies.

## V.2 Future Work

Considering all the exciting and impressive features, the AuBPs present abilities and capabilities worth to be further exploited in different fields of application. A few routes are envisioned as future perspectives based on what we have learned so far about these nanoparticles as follows:

- One path takes advantage of the AuBPs as active optical (nano)antennas, and proposes their implementation in the development of a dual read-out system that can provide qualitative and quantitative information for the detection of pesticides such as malathion, which affects the nervous system provoking thus sever health issues.

- We aim to take the paper-based plasmonic nanoplatform to the next level by incorporating multiple functionalities on the spatially isolated plasmonic line domains through their functionalization with molecules such as aptamers, which exhibit high specificity for the desired target analytes, thus, contributing to the progress of the nanotechnologies towards the design of innovative personalized fast miniaturized and portable biosensing devices.
- The further exploitation of the intrinsic PTT and/or PDT properties could lead to another route, specifically the design of devices with self-cleaning and self-sterilizing features arisen from the exposure of the integrated AuBPs to light sources.

# Dissemination of the results

## List of publications related to the doctoral thesis

### *Published papers in ISI journals*

***"ICG-loaded gold bipyramids towards their near-infrared PTT-PDT synergistic therapeutic potential in epithelial melanoma cells"***

**A. Campu**, M. Focsan, F. Lerouge, R. Borlan, L. Tie, D. O. Rugina, S. Astilean.

Colloids and Surfaces B:Biointerfaces Journal, 2020, 194, 111213

DOI: 10.1016/j.colsurfb.2020.111213.

Impact Factor 4.389, Article Influence Score 0.682.

***"Microfluidic Platform for Integrated Plasmonic Dual Detection"***

**A. Campu** , F. Lerouge, A. M. Craciun, T. Murariu, I. Turcu, S. Astilean, M. Focsan.

Nanotechnology, 2020, 31, 335502 DOI: 10.1088/1361-6528/ab8e72.

Impact Factor 3.551, Article Influence Score 0.706.

***"Assessment of the Photothermal Conversion Efficiencies of Tunable Gold Bipyramids under Irradiation by Two Laser Lines in NIR Biological Window"***

**A. Campu**, A. M. Craciun, M. Focsan, S. Astilean.

Nanotechnology, 2019, 30, 405701 DOI: 10.1088/1361-6528/ab2d90.

Impact Factor 3.551, Article Influence Score 0.706.

***"Multimodal Biosensing on Paper-Based Platform Fabricated by Plasmonic Calligraphy Using Gold Nanobipyramids Ink"***

**A. Campu**, L. Susu, F. Orzan, D. Maniu, A.M. Craciun, A. Vulpoi, L. Roiban, M. Focsan, S. Astilean.

Frontiers in Chemistry, 2019, V. 7, 55; DOI: 10.3389/fchem.2019.00055.

Impact Factor 3.693, Article Influence Score 0.869.

***"Gold NanoBipyramids Performing as Highly Sensitive Dual-Modal Optical Immunosensors"***

**A. Campu**, F. Lerouge, D. Chateau, F. Chaput, P. Baldeck, S. Parola, D. Maniu, A.M. Craciun, A. Vulpoi, S. Simion, M. Focsan.

Analytical Chemistry, 2018, V.90, P. 8567-8575; DOI: 10.1021/acs.analchem.8b01689.

Impact Factor 6.35, Article Influence Score 1.348

## *Manuscripts in preparation*

***"Gold Nanobipyramid-based SEIRA Immunosensor"***

**A. Campu** et al.

## Other Publications

## *Published papers in ISI journals*

***"Versatile Polypeptide-Functionalized Plasmonic Paper as Synergistic Biocompatible and Antimicrobial Nanoplatform"***

L. Tie, M. Răileanu, M. Bacalum, I. Codita, S. M. Negrea, C. S. Caracoti, E.-C. Drăgulescu, **A. Campu**, S. Astilean and M. Focsan.

Molecules, 2020, 25(14), 3182 DOI: 10.3390/molecules25143182.

Impact Factor 3.267, Article Influence Score 0.601.

***"Calligraphed Selective Plasmonic Array on Paper Platform for Complementary Dual Optical "ON/OFF Switch" Sensing"***

L. Susu, **A. Campu**, S. Astilean, M. Focsan.

Nanomaterials, 2020, 10(6), 1025 DOI: 10.3390/nano10061025.

Impact Factor 4.324, Article Influence Score 0.671.

***"Controlling the End-To-End Assembly of Gold Nanorods to Enhance the Plasmonic Response in Near Infrared"***

L. Tie, M. Focsan, J. Bosson, C. Tira, **A. Campu**, A. Vulpoi, S. Astilean.

Materials Research Express, 2019, 6, 095038 DOI: 10.1088/2053-1591/ab2eb0.

Impact Factor 1.929, Article Influence Score 0.229.

***"Designing Efficient Low-Cost Paper-Based Sensing Plasmonic Nanoplatforms"***

L. Susu*, **A. Campu***, A.M. Craciun, A. Vulpoi, S. Astilean, M. Focsan. (* These authors contributed equally to this work.)

Sensors, 2018, V. 18, 3035; DOI: 10.3390/s18093035.

Impact Factor 3.031, Article Influence Score 0.517.

***"A simple and efficient design to improve the detection of biotin-streptavidin interaction with plasmonic nanobiosensors"***

M. Focsan, **A. Campu**, C. Leordean, M. Potara, A. Gabudean, D. Maniu, S. Astilean.

Biosensors and Bioelectronics, 2016, V.86, P. 728-735; DOI: 10.1016/j.bios.2016.07.054.

Impact Factor 7.78, Article Influence Score 1.178.

## *Published papers in non-ISI journals*

***"Engineered Paper Platform loaded with Gold Nanospheres to improve SERS Performance for Analyte Detection"***

F. Orzan, **A. Campu**, S. Suarasan, S. Astilean, M. Focsan.

Studia UBB Physica, 2018, V. 63, 1-2, 143-152; DOI: 10.24193/subbphys.2018.15.

Impact Factor -, Article Influence Score -.

## *Published chapters in ISI journals*

***"Chapter 8. Advanced nanostructures for microbial contaminants detection by means of spectroscopic methods"***

M. Potara[*], **A. Campu[*]**, D. Maniu[*], M. Focsan[*], I. Botiz[*] and S. Astilean[*]

Elsevier 2020, Advanced Nanostructures for Environmental Health, Micro and Nano Technologies, Pages 347-384.

DOI: 10.1016/B978-0-12-815882-1.00008-2.

ISBN: 978-0-12-815882-1.

*All authors contributed equally to this work.

## Conference attendings

### *Oral presentations*

*5th International Workshop on Nano- and Biophotonics (IWNBP 2019), 22-27 September 2019, St Nectaire, France.*

***"Photothermal and Photodynamic Properties of ICG Containing Gold Bipyramids Towards their Therapeutic Potential in the NIR Biological Window"***

**A. Campu**, M. Focsan, D.O. Rugina, F. Lerouge, S. Parola, S. Astilean.

*Nanophotonics and Micro/Nano Optics International Conference Nanop 2018, 1-3 October, Rome, Italy.*

***"Enhanced multimodal biosensing using plasmonic paper-based nanoplatforms"***

**A. Campu**, F. Orzan, F. Lerouge, S. Parola, S. Astilean, M. Focsan.

*Gold 2018, 15-18 July 2018, Paris, France.*

***"Photothermal Therapy: optimal nanogold morphology for efficient heat generation"***

**A. Campu**, L. Susu, F. Lerouge, S. Parola, S. Astilean, M. Focsan.

*5th Edition of International Conference on Analytical and Nanoanalytical Methods for Biomedical and Environmental Sciences IC-ANMBES 2018, 23-25 Mai 2018, Brasov, Romania.*

***"Microfluidic Platform for Integrated Plasmonic Dual Detection"***

**A. Campu**, F. Orzan, T. Murariu, I. Turcu, I. Botiz, S. Astilean, M. Focsan.

*3rd International Workshop on Nano and Bio-Photonics, 6-11 December 2015, Cabourg, France:*

***"Sharp gold nanostructures for fluorescence enhancement"***

**A. Campu**, M. Focsan, F. Lerouge, P. Baldeck, S. Parola.

### *Poster presentations*

*Single-Molecule Sensors and nanoSystems International Conference, 3-5 April 2019, Munich, Germany.*

***"Gold Nanobipyramid-based SEIRA Immunosensor in Solution"***

**A. Campu**, D. Maniu, S. Astilean, M. Focsan.

*16th European Student Colloid Conference 2017, 19-22 June, Florence, Italy.*

***"Controlling the Assembly of Colloidal Gold Bipyramids for Dual-Modal Plasmonic Biodetection"***

**A. Campu**, M. Focsan, F. Lerouge, S. Parola, D. Maniu, S. Astilean.

*Molecular Plasmonics 2017, 18-20 May, Jena, Germany.*

*"**Gold Bipyramids performing as Dual-Modal Optical Immunosensors"***

**A. Campu**, M. Focsan, F. Lerouge, S. Parola, D. Maniu, S. Astilean.

*BioNanoSpec 2014, 7-10 September 2014, Cluj-Napoca, Romania.*

***"Raman Spectroscopy in Authenticity Studies, The discrimination of Inks and Stamps"***

**A. Campu** and N. Leopold

## *Conference contributions*

*5th International Workshop on Nano- and Biophotonics (IWNBP 2019), 22-27 September 2019, St Nectaire, France.*

**Invited Lecture**, ***"Calligraphed Plasmonic Paper Platforms for Multiplexed Detection"***

L. Susu, **A. Campu**, F. Lerouge, S. Parola, S. Astilean, M. Focsan.

**Invited Lecture**, ***"Designing Versatile Plasmonic-Based Nanoplatforms for Applications in Nanomedicine"***

S. Astilean, M. Potara, T. Simon, S. Suarasan, M. Focsan, A. Craciun, **A. Campu**, S. Boca-Farcau, C. Farcau, D. Maniu.

*Materials and Nanomaterials M&Ns-19, 17-19 July 2019, Paris, France.*

**Oral Presentation**, ***"Engineering Miniaturized Nanoplatforms via Plasmonic Calligraphy for Efficient Multimodal Biodetection"***

**A. Campu,** L. Susu, F. Orzan, L. Tie, S. Astilean, M. Focsan.

*Molecular Plasmonics 2019, 23-25 May, Jena, Germany.*

**Poster Presentation, *"Calligraphed plasmonic lines on paper operating as a miniaturized portable biosensing device"***

L. Șușu, **A. Câmpu**, S. Aștilean, M. Focșan.

*Sixth International Workshop on Advanced, Nano- and Biomaterials and Their Applications and Sixth French-Romanian Topical Meeting on Nano and Biomaterials, 12-16 May 2019, Cluj-Napoca, Romania.*

**Oral Presentation**, ***"Cysteine-Mediated Linear Assemblies of Gold Nanorods for Induced SERS Hot-Spots"***

L. Tie, J. Bosson, C. Tira, **A. Campu**, A. Vulpoi, S. Astilean, M. Focsan.

**Invited Talk**, ***"Designed Plasmonic-Based NanoSensors for Integrated Multimodal Biodetection"***

**A. Campu**, L. Susu, L. Tie, A. M. Craciun, F. Lerouge, S. Parola, S. Astilean, M. Focsan.

**Invited Talk**, ***"Plasmonic nanoplatforms for theranostic applications"***

M. Potara, T. Simon, S. Suarasan, M. Focsan, A. Gabudean-Craciun, S. Boca-Farcau, **A. Campu**, D. Maniu, S. Astilean.

*Nanophotonics and Micro/Nano Optics International Conference Nanop 2018, 1-3 October 2018, Rome, Italy.*

**Poster Presentation**, ***"Triple dyes-labeled polyelectrolyte microcapsules@gold nanoparticles for anthocyanins delivery as topical administration for tumor skin cells"***

R. Ghiman, D. Rugina, M. Focsan, **A. Campu**, A. Pintea, S. Astilean.

*Biosensors as tools for today's challenges, 23 July 2018, Bucharest, Romania*.

**Invited Lecture**, ***"Gold NanoBipyramids Performing as Highly Sensitive Dual-Modal Optical Immunosensors"***

**A. Campu**, L. Susu, S. Astilean, M. Focsan.

*Gold 2018, 15-18 July 2018, Paris, France.*

**Poster Presentation**, ***"Designing light-responsive nanogold-polyelectrolyte microsystems for controlled drug release in human retinal cells"***

Dissemination of the results

R. Ghiman, D. Rugină, **A. Campu**, M. Focsan, S. Astilean.

*NN18 15th International Conference on Nanosciences & Nanotechnologies, 3-6 July 2018, Thessaloniki, Greece.*

**Oral Presentation**, ***"Fabrication of innovative plasmonic paper-based nanosensors for label-free biodetection"***

**A.Campu**, L. Susu, F. Orzan, F. Lerouge, S. Astilean, M. Focsan.

*The Fifth Edition of International Conference on Analytical and Nanoanalytical Methods for Biomedical and Environmental Sciences IC-ANMBES 2018, 23-25 Mai 2018, Brasov, Romania.*

**Poster Presentation**, ***"Designing Efficient Low-Cost Paper-based Sensing Nanoplatforms"***

L. Susu, **A. Campu**, S. Astilean, M. Focsan.

**Poster Presentation**, ***"Controlling the End-to-End Assembly of Gold Nanorods to Enhance the Plasmonic Response in Near Infrared (NIR)"***

L. Tie, M. Focsan, C. Tira, **A.Campu**, A. Vulpoi, J. Bosson, S. Astilean.

*10th National Congress of Nefrology, 19-21 October 2017, Bucharest, Romania.*

**Poster Presentation**, ***"Plasmonic-microfluidic sensor for real-time on-site detection of ANCA antibodies"***

**A. Campu**, D. Maniu, S. Astilean, M. Focsan, F. Puskas, A. R. Potra, C. C. Rusu, D. T. Moldovan, I. M. Kacso.

*2nd International Conference on NanoMaterials for health, energy and enviroment, 7-11 September 2016, Flic en Flac, Mauritius.*

**Invited Lecture, *"Self-assembled Plasmonic Nanostructures for Ultrasensitive Detection"***

M. Focsan, **A. Campu**, A.M. Craciun, M. Potara, C. Leordean, D. Maniu, S. Astilean.

*7th International Conference on Metamaterials, Photonic Crystals and Plasmonics (META16), 25-28 July 2016, Torremolinos-Malaga, Spain.*

**Poster Presentation**, ***"Controlling fluorescence emission by surface plasmon resonance in multilayer "core-shell" metallic nanoparticles"***
M. Focsan, **A. Campu**, A. Craciun, S. Suarasan, C. Tira, A. Lazar, S. Astilean.

*3rd International Workshop on Nano and Bio-Photonics, 6-11 December 2015, Cabourg, France.*
**Invited Lecture**, ***"Plasmonic Platforms for Ultrasensitive Detection"***
M. Focsan, **A. Campu**, S. Suarasan, A. Gabudean, M. Potara, D. Maniu, S. Astilean.

*3rd International Conference on BioPhotonics 2015, 20-22 May 2015, Florence, Italy.*
**Poster Presentation**, ***"Senzitivity improved Plasmonic Platform for specific Biomarkers Detection"***
M. Focsan, **A. Campu**, C. Leordean, M. Potara, A. Gabudean, D. Maniu, S. Astilean.

## Patent application related to the doctoral thesis

Patent Application Nr. A 2018 00958
***„Dispozitiv microfluidic plasmonic pe bază de nanoparticule bipiramidice de aur"***
M.Focsan, **A. Campu**, S. Astilean, T. Murariu, I.Turcu.

## Awards

**Procter&Gamble Award:** ***Best Poster Among Women in Science 2017***.

## Teaching activity

**2019 – 2020:** Teaching **Optics laboratories** for 1st year Chemistry Students at the Faculty of Physics, Babes-Bolyai University

## Specialization courses and training

03 – 11 November 2016: ***Training in the Functional Materials Team of the Chemistry Laboratory, École Normale Supérieure of Lyon and Université Lyon 1***, Lyon, France.

29 November – 09 December 2017: ***Training at the CSPBAT Laboratory,*** **Paris 13 University**, Paris, France.

Dissemination of the results

06 – 08 March 2018: ***10th European short course on "Time-Resolved Microscopy and Correlation Spectroscopy"***.

09 March 2018: ***18th SymPhoTime Training Day – "Hands-on Data Analysis"***.

## Funding and grants

### *Grants awarded by competition*

**Ministry of Research and Innovation, CNCS-UEFISCDI – as Project Director**, under de project number: ***Mobility Project for Researchers***, project number **PN-III-P1-1.1-MC-2017-3573.**

### *Member in research projects*

**Ministry of Research and Innovation, CNCS-UEFISCDI – as Member 10 in Research Projects.**

Appendix 3

# Acknowledgements

*"Give a man a fish and you will feed him for a day.*
*Teach a man how to fish and you feed him for a lifetime."*
(Old proverb)

Over the past few years, I have received the conscious and unconscious help and support from a lot of people, who, as the old saying implies, have not only shown me the way, but teached me how to walk it. These years have significantly contributed to my professional and personal self-development.

First and foremost, I would like to acknowledge and give my deepest thanks to my family, my mother and brother, who have been my biggest supporters throughout my entire life, the ones to call when happiness was to be shared and when tears were to be shed. Their unconditional trust, support and love have made me who I am today (along with the occasional incentives, to be fair) and I cannot express through words how deeply they are appreciated.

I would like to thank my closest friends for their support and constant encouragement, for believing in me and being there regardless of time and distance. Thank you!

My gratitude is expressed towards my coordinator, prof. Simion Astilean, who has offered me the opportunity to learn and work in his highly experienced research group. His support and advices as well as craving for knowledge have helped me grow and improve. Despite the sometimes-challenging communication, the messages have always reached their destination knowing they were sent for my best. Therefore, I can only hope I have met the expectations and, maybe, even reached beyond them.

The best gift was to meet my mentor, Habil. Dr. Monica Focsan, whom I actively worked with and learned from. There are strangers in life who become your acquaintances and then your friends. However, the most valuable people in life are those you get to acknowledge as a family. Her unconditioned trust and support have left their marks not only on my scientific achievements, but also on my personal progress boosting my confidence and helping me become self-aware of my own strength and capabilities. I am deeply grateful for the opportunities she has offered and shared with me; we do make a great team. If only there were more people like you! Thank you from the bottom of my

heart for your patience and for “letting me be me”! Thank you for everything! I hope I have made you proud!

I would like to thank Assoc. Prof. Dr. Frederic Lerouge for the help and support offered throughout these years, for the time spend answering my (sometimes stupid) chemistry questions. Thank you for your encouragements, advocacy and trust, it made a consistent difference for me both professionally and personally and I truly appreciate you for that and not only.

To my colleagues from the Nanobiophotonics and Laser Microscopy Center, your companionship has created a pleasant and fun working environment. Thank you for the constructive talks (no matter the subject), late (but fun) work nights and your friendship inside and outside the walls of the laboratory.

Lastly, I would like to acknowledge all the people who have effectively contributed to this work as well as to the advisory board for all the constructive comments and advices.

**Thanks to all who have taught me how to fish as I am grateful to you for a lifetime.**